# Behaviours of pyroclastic and analogue materials, in dry and wet environments, for use in experimental modelling of pyroclastic density currents

WALDING, Nemi <http://orcid.org/0000-0002-4584-1319>, WILLIAMS, Rebecca <http://orcid.org/0000-0002-8203-9982>, ROWLEY, Pete <http://orcid.org/0000-0002-8322-5808>, DOWEY, Natasha <http://orcid.org/0000-0002-9231-4781>, PARSONS, Daniel and BIRD, Anna <http://orcid.org/0000-0002-2496-4344>

RESEARCH ARTICLE

VOLCANICA

# Behaviours of pyroclastic and analogue materials, in dry and wet environments, for use in experimental modelling of pyroclastic density currents

Nemi Walding*[α,β], Rebecca Williams[β], Pete Rowley[γ], Natasha Dowey[δ], Dan Parsons[ε], and Anna Bird[β]

[α] Energy and Environment Institute, University of Hull, Hull, UK.
[β] School of Environmental Sciences, University of Hull, Hull,UK.
[γ] School of Earth Sciences, University of Bristol, Bristol, UK.
[δ] Geography, Environment and Planning, Sheffield Hallam University, Sheffield, UK.
[γ] Loughborough University, Loughborough, UK.

Submitted: 2024-04-15 | Accepted: 2024-09-27 | Published: 2025-05-15

Editor: J. Farquharson | Typesetter: G. Seropian

## Abstract

Modelling pyroclastic density currents (PDCs) is a challenging yet essential element of hazard assessment. PDCs are unpredictable and internal processes are often difficult to measure directly. Analogue experiments have been an important tool for investigating internal PDC dynamics. Typically, analogue experiments have removed moisture from experimental materials to limit cohesion. However, this does not represent natural systems well, where moisture can be introduced into a PDC through a variety of processes. In this study, we characterise pyroclastic and analogue materials in dynamic (i.e. flowing), static (i.e. stationary), wet and dry experiments to explore fundamental frictional and fluidisation behaviours. The addition of moisture can lead to changes in material properties resulting in significant impacts on geomechanical behaviours (size, density, shear strength), fluidisation and flowability. This work highlights the importance of validating the material choice used in modelling experiments, especially in wet conditions.

## Resumen

La modelización de las corrientes de densidad piroclástica (PDCs) es un elemento difícil pero esencial de la evaluación de riesgos. Las PDCs son impredecibles y los procesos internos suelen ser difíciles de medir directamente. Los experimentos análogos han sido una herramienta importante para investigar la dinámica interna de las PDCs. Normalmente, los experimentos análogos han eliminado la humedad de los materiales experimentales para limitar la cohesión. Sin embargo, esto no representa bien los sistemas naturales, en los que la humedad puede introducirse en un PDC a través de diversos procesos. En este estudio, caracterizamos materiales piroclásticos y análogos en experimentos dinámicos (es decir, fluidos), estáticos (es decir, estacionarios), húmedos y secos para explorar comportamientos fundamentales de fricción y fluidización. La adición de humedad puede provocar cambios fundamentales en las propiedades de los materiales, lo que tiene importantes repercusiones en los comportamientos geomecánicas (tamaño, densidad, ángulo de fricción interna), la fluidización y la fluidez. Este trabajo pone de relieve la importancia de validar la elección del material utilizado en los experimentos de modelización, especialmente en condiciones de humedad.

Keywords: Cohesion; Fluidisation; Erosion; Substrate; Volcaniclastics; Volcanology.

## 1 Introduction

A pyroclastic density current (PDC) is a volcanic hazard formed during explosive eruptions and dome collapse events. PDCs are rapidly moving, high temperature (up to 1000°C) currents of heterogeneous volcanic material and gas [Fisher 1979; Cas and Wright 1988; Branney and Kokelaar 2002; Dufek 2016]. They are multiphase flows, where the solid, granular phase consists of both juvenile and entrained material, and the fluid phase contains a combination of volcanic gas and vapour with entrained air [Burgisser et al. 2005; Esposti Ongaro et al. 2011; Esposti Ongaro et al. 2012; Lube et al. 2020].

Internal dynamics within PDC systems are difficult to observe in real time. In-situ data are rare, flows can be unpredictable, and equipment can be damaged by extreme force [Wilson et al. 2014; Scharff et al. 2019]. The behaviour of PDCs, including flow runout distance, duration and velocity, is collectively controlled by variations in flow parameters such as mass flux, particle size, particle shape, density, fluid medium and changes in topography [Bursik and Woods 1996; Branney and Kokelaar 2002]. Particle size variations, including ash (<2 mm) concentration, can be attributed to various factors, including magma composition, fragmentation rate, amount and duration, initial vent dynamics, erosion and sedimentation processes during flow propagation, and current vertical density segregation [Sparks 1976; Zimanowski et al. 1997; Alidibirov and Dingwell 2000; Branney and Kokelaar 2002; Dufek and Manga 2008; Breard et al. 2023]. Particle density contrast can be driven by variation in mixture composition and vesicularity and can lead to further vertical and lateral particle segregation [Doyle et al. 2010]. Finally, the temperature and fluid medium (gas or water) in PDCs can con-

* nwalding@kelpiegeoscience.com

tribute to the generation of pore pressure or other controls on interparticle forces, fundamentally affecting particle and bulk material behaviour [Druitt et al. 2007; Lube et al. 2020]. Understanding these complex variations is crucial for exploring the dynamics of PDCs.

Advances in the understanding of PDCs have been driven by a multi-method approach of direct observation [e.g. Cole et al. 1998; 2002; Lipman 2018; Vecino et al. 2022], detailed geological stratigraphy [e.g. Fisher 1979; Branney and Kokelaar 1997; Brown et al. 2003; Brown and Branney 2013; Douillet et al. 2013; Smith and Kokelaar 2013; Douillet et al. 2018], small and large scale analogue experiments [e.g. Dellino et al. 2007; Rowley et al. 2014; Lube et al. 2015; Smith et al. 2018; Lube et al. 2019; Smith et al. 2020; Walding et al. 2023] and numerical modelling [e.g. Valentine 1987; Dufek 2016; Kelfoun et al. 2017; Breard et al. 2018]. Analogue experiments validate data and underpin the basic geophysical properties that can then be used to generate new or update existing numerical models.

The most common materials used in PDC analogue modelling are soda-lime glass ballotini (microspheres/glass beads). This is due to their widespread availability, narrow and well-defined size distribution, and consistent physical properties [e.g. Roche et al. 2004; Chedeville and Roche 2014; Rowley et al. 2014; Smith et al. 2018; Gilbertson et al. 2020]. However, when trying to simulate the behaviour of polydisperse and non-spherical natural pyroclastic materials, the uniformity of ballotini is not ideal. Given the importance of particle characteristics in controlling frictional behaviours and permeability, the choice of material for analogue experimentation is critical, and yet no known studies have directly compared the behaviour of analogue material to a range of natural pyroclastic samples under both static and dynamic conditions. Recent work has shown the powerful impact of even small (<1 wt.%) moisture contents on the fluidisation behaviours of pyroclastic sediments [Walding et al. 2023]. This work sets out to quantify the static (i.e. motionless material) and dynamic (i.e. material undergoing changes in motion over time) behaviours of various pyroclastic and analogue materials in dry and "wet" (>0 wt.% water) environments, for use in analogue modelling. The work aims to investigate the geomechanical behaviours of these materials, to both establish a baseline for material variability under these different conditions (i.e. a flowing current, a stationary substrate or as a defluidising deposit), and to determine the most suitable material for simulation of different natural PDCs. This work adopts the same methodological approach as Walding et al. [2023], expanding the range of pyroclastic material tested and directly comparing behaviours to a range of analogue material.

### 1.1 Material selection in experimental PDC modelling

A variety of analogue materials can be used in experimental modelling to mimic the behaviours of natural material. The choice of analogue materials used in PDC modelling is often justified for their fluidisation properties. Fluidisation plays an important role in PDC mobility [Sparks 1976; 1978; Wilson 1984; Branney and Kokelaar 1992; 2002; Roche 2012; Breard and Lube 2017; Aravena et al. 2021; Breard et al. 2023; Salatino et al. 2024] and the formation of deposit structures resulting from defluidisation and degassing [i.e. gas escape structures; Wilson 1980; Cas and Wright 1991; Pacheco-Hoyos et al. 2020; Walding et al. 2023]. The upward movement of gas can support particles within the flow, opposing the forces of gravity, and reducing contact friction.

The fluidisation of pyroclastic materials can be assessed through experimental set-ups such as the use of fluidisation columns [Wilson 1984; Roche et al. 2001; Bareschino et al. 2007; Gilbertson et al. 2020; Walding et al. 2023], rotating drums [Valverde and Soria-Hoyo 2015; Smith et al. 2020; Walding et al. 2023] or flumes [Roche et al. 2004; Dellino et al. 2007; 2010; Roche 2012; Lube et al. 2015; Smith et al. 2018; Brosch et al. 2021]. Additionally, the use of numerical modelling can simulate the behaviour of PDCs under different conditions [Esposti Ongaro et al. 2002; Dartevelle et al. 2004; Benage et al. 2016; Kubo Hutchison and Dufek 2021]. Observations of PDC deposits in the field offer valuable insights into evidence of PDC fluidisation behaviours. This can be through evidence of gas escape in deposits [Fisher and Schmincke 1984; Cioni et al. 2015; Pacheco-Hoyos et al. 2020] or by observations of recently deposited material [Whelley et al. 2012].

Using the Geldart [1973] classification, pyroclastic materials can be categorised based on their fluidisation behaviour. Geldart [1973] separated powders into four distinct groups (A–D), differentiated by their fluidisation behaviours, where powders can exhibit a "very poor" to "excellent" fluidisation state, based on particle size, shape and density. Group A (30–100 µm) and Group B (100 µm–1 mm) powders tend to uniformly expand during fluidisation, and often display the most favourable fluidisation behaviours (e.g. homogeneous bubbling and channelling). In contrast, the finest particles (<20 µm) in Group C are dominated by the presence of interparticulate forces (e.g. electrostatic cohesion and Van der Waals) and therefore fluidisation behaviours are usually poor. Group D (>1 mm) particles are the largest and require overall higher gas velocities for effective fluidisation. Group D has moderate to poor fluidisation and often demonstrates slugging, channelling, and spouting behaviours [Leturia et al. 2014].

To match the fluidisation behaviours of PDCs, and to minimise variability in other particle parameters such as shape, density, and roughness, the most common analogue material used to date are ballotini beads, commonly Geldart Groups A and B (Table 1). Using mean particle diameters below ~150 µm generally ensures these materials can easily fluidise at gas velocities achievable in the laboratory [Roche et al. 2004; Montserrat et al. 2012; Rowley et al. 2014; Breard et al. 2019]. The benefit of using ballotini is that, as well as its excellent fluidisation behaviours, it is widely available for use. However, it does not capture the full particle variability of natural pyroclastic material.

Pyroclastic material has been used in small-scale experiments, to investigate modelling of gas escape structures and in geomechanical tests to explore material strength and flow behaviours [Roche et al. 2001; 2004; Smith et al. 2018; Smith et al. 2020; Osman et al. 2022; Walding et al. 2023]. However, the large polydispersity can lead to issues such as scaling lim-

Table 1: Compilation of published works on material properties of analogue and pyroclastic material used in experimental modelling. The values represent the properties of the material used in a range of static and dynamic studies. SAoR—Static Angle of Repose, DAoR—Dynamic Angle of Repose.

| Literature | Sample | Experiment type | Mean size (mm) | Median size (mm) | Size range (mm) | Fines content (%) | Density (kg m$^{-3}$) | SAoR (°) | DAoR (°) | Friction angle (°) |
|---|---|---|---|---|---|---|---|---|---|---|
| Roche et al. [2004] | Ballotini | Dynamic (Flow) | – | – | 0.024–0.090, 0.106–0.212, 0.6–0.8 | – | 1492, 1467, 1450 | 28.5, 24.5, 24 | – | – |
| Dellino et al. [2007, 2010] | Somma Vesuvius Pyroclastic Deposits | Dynamic (Flow) | – | 1 | 0.011–8 | – | 1630 | – | – | – |
| Lube et al. [2015] | Taupō Ignimbrite Mixture | Dynamic (Flow) | – | 241–366 | 0.0014–22 | 4.5–17 | 400–2600 | – | – | – |
| Smith et al. [2020] | Ballotini | Static and Dynamic | 0.0634 | – | 0.045–0.090 | – | 1450–1740 | 10–34 | 14–26 | – |
| Smith et al. [2020] | Pozzolane Rosso Ignimbrite | Static and Dynamic | 0.018–0.7 | – | 0.003–3 | – | – | 31–61 | 39–53 | – |
| Breard and Lube [2017], Brosch et al. [2021] | Taupō Ignimbrite Mixture | Dynamic (Flow) | – | – | 0.002-16 | 20 | 350–2600 | 39 | – | – |
| Osman et al. [2022] | Industrial Pumice (Synthetic) | Static | 0.063 | – | – | – | 602–412 | – | – | 36.5 |
| Osman et al. [2022] | Ascension Ash | Static | 0.063 | – | – | – | 1019 | – | – | 36.4 |
| Vale et al. [2024] | Glass Ballotini | Static | – | – | 1–1.4 | – | 2500 | – | – | – |
| Vale et al. [2024] | Crushed Pumice | Static | – | – | 0.5–2.0 | – | 1080 | – | – | – |
| Vale et al. [2024] | Ruapehu Ash | Static | – | – | 0.5–2.0 | – | 2200 | – | – | – |

itations (i.e. having a maximum size range to fit within the limits of experimental apparatus and jamming in small-scale hoppers) and behavioural challenges associated with fluidisation (i.e. large particle polydispersity leading to issues in homogeneous fluidisation of material) [Wilson 1984; Walding et al. 2023]. Some of these issues can be alleviated by using large-scale flow experiments [Dellino et al. 2007; 2010; Lube et al. 2015; Brosch et al. 2021, Table 1]. Additionally, variables introduced by using pyroclastic material (i.e. particle size distribution, particle density, roughness, composition, etc.) can lead to added degrees of complexity when modelling using natural pyroclastic materials. Furthermore, it is difficult to get large, homogenous samples of natural materials and in certain areas of the world challenges can arise when trying to obtain natural samples. The nature of each individual sample of material can vary greatly due to changes in sample type (i.e. location of material and volcano), eruption dynamics and age (e.g. weathering and alteration). However, the use of natural pyroclastic material in experimental modelling is a fundamental step in understanding natural processes and how these vary from the behaviours of analogue material.

Previous studies [such as Breard et al. 2019; Smith et al. 2020; Osman et al. 2022; Walding et al. 2023; Vale et al. 2024] have explored the use of analogue versus natural material to begin to characterize properties such as material behaviour, shear strength, flowability, fluidisation and permeability. Ballotini [Roche et al. 2004; Smith et al. 2020; Vale et al. 2024] and crushed industrial pumice [Osman et al. 2022; Vale et al. 2024] has been used in a wide range of analogue studies. However, when using natural pyroclastic material it is often the case that only small amounts of natural material is used from single eruptions (e.g. 232 AD Taupō ignimbrite [Breard et al. 2019]; Ascension tephra [Osman et al. 2022]; andesitic ash sample from Ruapehu [Vale et al. 2024]) against which to compare analogue materials. Table 1 collates published works of both analogue and pyroclastic material behaviour used in static and dynamic conditions. In this study, we expand on these exploratory results to investigate the geomechanical behaviours of a wider suite of pyroclastic and analogue material through static, dynamic, dry and wet conditions. Furthermore, we expand on work by Walding et al. [2023] and begin to further investigate the role of water on a suite of pyroclastic material.

### 1.2 Moisture in a PDC system

Moisture, in the form of water vapor or liquid water, can enter a PDC system during its formation, often due to water-rich environments from phreatomagmatic interactions, during its propagation or during and after deposit aggradation. This introduction of moisture can result from a combination of atmospheric conditions [e.g. humidity, Pepin et al. 2017; Camuffo 2019], topographic factors [e.g. elevation, Barclay et al. 2006; Duane et al. 2008; Hartmann 2016], and meteorological conditions (e.g. precipitation). Furthermore, PDCs can interact with external bodies of water such as streams, lakes, the sea, and snow [Cole et al. 1998; 2002; Dartevelle et al. 2004; Vale et al. 2024], as well as water-saturated substrates [Moyer and Swanson 1987; Brown and Branney 2013; Gilbertson et al. 2020].

The temperature within a PDC system can vary widely. Low temperature (<100°C) currents are interpreted to form from phreatomagmatic interactions [Sparks and Wilson 1990; Yamamoto et al. 1999] while high temperatures are interpreted to reach in excess of 700 °C [McClelland and Druitt 1989; Bardot 2000; Cioni et al. 2004; Lesti et al. 2011; Pensa et al. 2023]. Near the surface and in the upper parts of the flow, pressures may be close to atmospheric and temperatures cooler, whereas in the denser parts of PDCs, both pressures and temperatures can increase significantly [Breard and Lube 2017]. Changes in these conditions can lead to the condensation of water vapour into droplets. As a result, the moisture content in PDCs and their resultant deposits can vary in both time and space. For example, the rapid vaporization of water into steam during granular PDC interactions with wet substrates can create a new gas source, increasing the mobility and fluidisation of the current, whereas moisture influence from precipitation and atmospheric conditions may be more likely to affect the dilute regime of the current.

### 1.3 The influence of moisture on experimental modelling materials

When conducting analogue experiments to model PDCs, procedures are often implemented to minimize the moisture content of the material used. This typically involves drying samples in an oven for 24 hours, which helps to remove adsorbed moisture and reduce the effects of cohesion. However, volcanic eruptions and tephra plumes may include a high proportion of water vapour, either from phreatic or phreatomagmatic eruption processes or from entrainment of moisture from the atmosphere and environment [Self and Sparks 1978; Morrissey and Mastin 2000; Van Eaton and Wilson 2012; Pardo et al. 2014]. This can lead to moisture-rich PDCs forming at source. Additionally, moisture can be incorporated into the flow as a PDC propagates, even if initially dry, e.g. from rainfall into the current, travelling over water bodies, or encountering moisture-rich substrates such as vegetation or wet soils [Walding et al. 2023, and references therein].

Walding et al. [2023] explored the behaviour of small quantities of moisture on fine pyroclastic material (≤1000 µm). The findings revealed that the introduction of water (>0.50 wt.%) into pyroclastic material can significantly change the cohesive properties, which in turn alters the flowability from a free flowing to a non-flowing material. This is due to the friction coefficient increasing due to the formation of capillary bridges. Results also demonstrated that changes in moisture content could significantly affect fluidisation profiles and resulting gas escape structures forming within a deposit. Fluidisation experiments of the material showed gas bubbling throughout most experiments (with minimum bubbling velocity $U_{mb}$ ), with gas bubbles rising from the basal gas supply [Walding et al. 2023]. With increasing gas flux, or in more polydisperse mixtures, gas escape can lead to channelling (with minimum velocity to induce channelling $U_{mc}$ ), where gas pathways are concentrated into vertical channels (approaching Geldart Group D behaviours). With the introduction of water (> 0.50 wt.%), drying profiles migrate through the moist deposit and can form areas of wet lobes and bubbling dry pockets

[Walding et al. 2023]. Explosive channelling (with minimum velocity to cause gas escape feature formation $U_{mx}$ ) is also observed in experiments of 0.50-5.00 wt.% water. This is where the material dries, and an upper wet deposit inhibits gas escape leading to a pressure increase and subsequent release. Finally, under the highest moisture conditions, pressure builds under the moist deposit until the deposit fractures into cracks ($U_{mcr}$) where gas can then easily permeate through. This work highlights the impacts of water on pyroclastic material and demonstrates the need to further explore the role of water on PDC flow dynamics and deposit behaviour.

There is a notable gap in research into the behaviours of a range of pyroclastic and analogue materials across static and dynamic experiments, particularly in dry versus wet environments. This lack of comprehensive study may lead to inadequate experimental design, and it is therefore imperative to enhance our understanding of these behaviours. Doing so will facilitate the validation of analogue materials utilized in experimental modelling and enable the exploration of fundamental characteristics of natural pyroclastic materials. In these experiments we aim to look at pyroclastic material behaviour in the presence of moisture. These observed behaviours can then be used to infer implications for PDC systems, from flow to deposit.

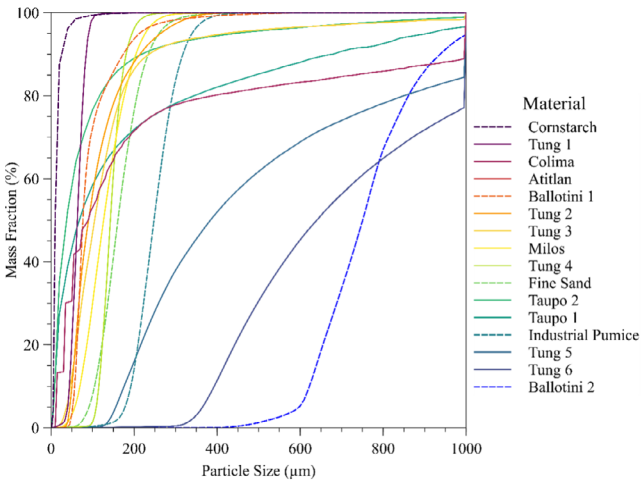


Figure 1: Grain Size Distribution (GSD) plot of pyroclastic (solid line) and analogue (dashed line) materials used throughout the experiments. Materials in legend are organised by logarithmic particle size mean (with cornstarch the finest grained material used) (Φ) for this and subsequent figures.

## 2 Methods and materials

The experimental methods within this paper follow those used in Walding et al. [2023] and are summarised here. More detailed descriptions of the methods used are detailed in Supplementary Material A.

### 2.1 Pyroclastic and analogue samples

Five natural samples of pyroclastic material were chosen to cover a range of physical particle size characteristics (size, shape, fines content; Table 2). Samples were collected from a variety of global locations and represent different eruption styles, lithofacies and geochemical compositions (Table 2). The analogue samples include material that has previously been used in experimental modelling of pyroclastic behaviours (ballotini [Roche et al. 2004; Smith et al. 2018; Smith et al. 2020] and exploratory samples (i.e. cornstarch, Table 3). The pyroclastic samples have maximum particle diameters of 2000 µm and the analogue samples have maximum particle diameters of 1460 µm (Figure 1). These size ranges were chosen to accommodate the scaling limits of the fluidisation chamber experiments.

#### 2.1.1 *Scaling*

The work presented here arises from questions about how volcanic materials physically respond to moisture. Although it would be straightforward to analyse natural samples and measure their mechanical response to moisture changes, experimental simulations of natural processes, such as PDC propagation, often utilize various analogous materials instead of pyroclastic sediment. To support this study, we tested a range of these analogue materials alongside natural pyroclastic ones, with the hope that this data will be useful for future research on how these characteristics influence processes within currents, deforming sediments, and other related phenomena.

The scaling of experiments depends on the specific conditions and apparatus design. Therefore, we provide a list of key parameters for each of our tested materials (Table 4). The experiments discussed here examine the mechanical properties of the entire material, though there are limitations, notably, the particle sizes used are restricted to the ash fraction (<2 mm). This limitation is due to the apparatus, which requires a minimum number of particle diameters to produce repeatable and meaningful data. In natural settings, the particle size distribution can be much broader, which may have impacts on the mechanical properties we are unable to quantify here.

#### 2.1.2 *Wetting process*

To ensure the removal of residual absorbed moisture in the experiments, all samples were dried for 24 hours at 80°C. Any agglomerations were broken-up by sieving prior to the start of the experiments. For the moisture tests, water was then added to the samples based on weight percentage (0, 0.25, 0.50, 1.00, 2.50, 5.00 wt.%). These moistures were chosen as they have been identified in Walding et al. [2023] as being significant in affecting the cohesive behaviour and the resulting shear strength of material. Samples were mixed thoroughly to ensure a homogeneous moisture distribution [Walding et al. 2023].

### 2.2 Particle size and shape analysis

Particle analysis of the pyroclastic and analogue material was undertaken using a CAMSIZER X2, which uses particle imaging to establish shape and size characteristics for dry material samples. The CAMSIZER provides a maximum resolution of 0.8 µm per pixel for both particle size and shape. We report

Table 2: Pyroclastic samples used in the reported experiments, reporting formation processes, chemical composition, location of sample collection and references (where applicable).

| Material | Eruption/Formation | Composition | Location | References |
|---|---|---|---|---|
| Tung (1–6) | 2006 VEI 3 eruption. Sieved PDC units sampled by U. Kueppers in 2009. | Andesitic | Tungurahua, Ecuador | Kelfoun et al. [2009], Eychenne et al. [2012], Douillet et al. [2013], Hall et al. [2013] |
| Colima | 2015 eruption. Sieved PDC units sampled by T. Johnson in 2023. | Andesitic | Volcán de Colima, Mexico | T. Johnson [pers. comm., 2023] |
| Atitlán | Unstudied ignimbrite deposit. Sampled by P. Rowley from massive PDC unit in 2023. GR: 14°40'55.24"N, 91°15'29.15"W | – | Volcán de San Pedro, Guatemala | P. Rowley [pers. comm., 2023] |
| Taupō (1 & 2) | Taupō 1: Sampled from the proximal fine ash-rich facies from the base of 232 AD deposit. Taupō 2: Sampled from 232 AD proximal PDC deposits. Sampled by E. Brosch and colleagues. | Rhyolitic | Taupō, New Zealand Taupō 1: 17 km from vent Taupō 2: 8 km from the vent | Wilson [1985], Brosch et al. [2021] |
| Milos | Basal pyroclastic sequence. PDC units sampled by N. Walding in 2023. | Rhyolitic to Dacitic | Milos, Greece | Zhou et al. [2021] |

Table 3: Analogue samples used in the experiments. Ballotini 1 and 2 represent the size variation of the two material samples used.

| Material | Composition | Material Information |
|---|---|---|
| Ballotini (1 & 2) | Soda lime glass beads | Sourced from `sandblasters.co.uk` |
| Fine Sand | Redhill 110 (silica sand) | Sourced from `mineralsmarketing.co.uk` |
| Cornstarch | Cornstarch | Sourced from Harry Harvey Ltd© |
| Industrial Pumice | Unspecified pumice | Sourced from Specialist Aggregates Ltd® |

particle sphericity SPHT values using [Liu et al. 2019]:

$$\mathrm{SPHT} = \frac{4\pi A P}{U^2}, \tag{1}$$

where $P$ is the measured circumference of the particle and $A$ is the area covered by particle projection. For an ideal sphere, SPHT is expected to be 1, otherwise it is smaller than 1 [Liu et al. 2019].

Symmetry is measured by how evenly the shape of a particle is distributed around the centre line. For example, asymmetric particles will be <1. The cumulative size and shape data from CAMSIZER were subsequently processed using GRADISTAT [Blott and Pye 2001] to derive various particle size characteristics, using the moments method [Inman 1952] to calculate logarithmic and geometric particle size mean $\bar{x}$ (Φ), median (Φ), range (µm), sorting index σ (Φ), sorting $\sigma_G$, skewness $Sk$ (Φ), kurtosis $K$ (Φ), and the geometric mean (µm). The Sauter mean diameter $D_{32}$ is a measurement that describes the diameter of a sphere that has the same volume to surface area ratio of a particle [Breard et al. 2019]:

$$D_{32}(\mathrm{mm}) = 2^{-\left[\mu_m(\Phi)+\frac{\ln 2}{2}\sigma^2(\Phi)\right]}, \tag{2}$$

where $\mu_m$ is the geometric mean and σ is the geometric standard deviation [both in Φ units, Breard et al. 2019]. $D_{32}$ values have been used to characterise the fluidisation behaviour of a material [Breard et al. 2019]. Following the approach outlined in Breard et al. [2019], we calculated the $D_{32}$ (mm) and fines content (<63 µm, %) of the material.

8(1): 261–285. https://doi.org/10.30909/vol/oxkm9163

Table 4: Material properties of both pyroclastic (sample names shaded dark grey below) and analogue materials (shaded pale grey). These include logarithmic particle size mean and particle size median, particle range, fines content (Fines Cont., <63 µm), geometric mean (Geom. Mean, Φ), and employ the method of moments for calculating mean, sorting, sphericity SPHT, symmetry (Symm.), skewness $Sk$, and kurtosis $K$. The Sauter mean diameter $D_{32}$ is computed following the methods outlined in Breard et al. [2019]. Additionally, the Geldart Groups Classification [Geldart 1973] is determined based on the logarithmic mean particle size. Table is ordered by logarithmic particle size mean.

| Material | Particle Size Mean $\bar{x}$ (Φ) | Particle Size Median (Φ) | Particle Size Range (µm) | Fines Cont. (%) | Sorting Index σ (Φ) | Sorting $\sigma_G$ | SPHT | Symm. | $Sk$ (Φ) | $K$ (Φ) | $D_{32}$ (mm) | Geom. Mean (µm) | Geldart Groups |
|---|---|---|---|---|---|---|---|---|---|---|---|---|---|
| Corn Starch | 4.82 | 4.83 | 5–340 | 96.17 | 0.60 | Moderately Well Sorted | 0.84 | 0.91 | -0.30 | 4.32 | 0.02 | 35.4 | A, B, C |
| Tung 1 | 3.78 | 3.73 | 2.5–297 | 35.76 | 0.43 | Well Sorted | 0.77 | 0.88 | 1.89 | 17.00 | 0.06 | 72.9 | A |
| Colima | 3.46 | 3.62 | 10–1000 | 84.39 | 1.45 | Poorly Sorted | 0.72 | 0.86 | -0.51 | 2.56 | 0.04 | 90.3 | A, B, C |
| Atitlán | 3.44 | 3.83 | <20–1780 | 66.03 | 1.50 | Poorly Sorted | 0.83 | 0.91 | -0.91 | 3.17 | 0.02 | 92.4 | A, B, C, D |
| Ballotini 1 | 3.43 | 3.61 | 20–655 | 14.78 | 0.62 | Moderately Well Sorted | 0.90 | 0.93 | -0.46 | 4.72 | 0.08 | 92.7 | A, B, C |
| Tung 2 | 3.22 | 3.32 | 15–425 | 15.32 | 0.71 | Moderate | 0.79 | 0.86 | -0.52 | 2.58 | 0.01 | 107.5 | A, B |
| Tung 3 | 3.12 | 3.14 | 5–1000 | 19.25 | 0.87 | Moderate | 0.74 | 0.84 | -0.56 | 4.14 | 0.01 | 115.0 | A, B |
| Milos | 2.92 | 2.87 | 15–615 | 8.69 | 0.56 | Moderately Well Sorted | 0.74 | 0.84 | 0.47 | 3.34 | 0.06 | 132.4 | A, B, C |
| Tung 4 | 2.70 | 2.71 | 20–650 | 0.15 | 0.25 | Very Well Sorted | 0.84 | 0.87 | 0.14 | 8.54 | 0.01 | 153.5 | A, B |
| Fine Sand | 2.57 | 2.55 | 10–530 | 0.84 | 0.44 | Well Sorted | 0.86 | 0.88 | 0.38 | 4.64 | 0.14 | 168.7 | A, B, C |
| Taupō 2 | 2.35 | 2.37 | <20–2000 | 52.23 | 0.98 | Moderately Sorted | 0.70 | 0.86 | -0.48 | 4.06 | 0.04 | 195.8 | A, B, C, D |
| Taupō 1 | 2.08 | 2.20 | <20–2000 | 38.90 | 1.16 | Poorly Sorted | 0.75 | 0.87 | -0.50 | 3.33 | 0.04 | 234.6 | A, B, C, D |
| Industrial Pumice | 1.81 | 1.77 | 5–1000 | 0.07 | 0.99 | Moderately Sorted | 0.79 | 0.87 | 0.80 | 4.51 | 0.24 | 284.0 | A, B, C |
| Tung 5 | 1.51 | 1.57 | 10–1000 | 0.09 | 0.76 | Moderate | 0.80 | 0.87 | -0.10 | 2.48 | 0.02 | 347.3 | A, B |
| Tung 6 | 0.83 | 0.81 | 10–1000 | 0.04 | 0.45 | Well Sorted | 0.79 | 0.87 | 0.59 | 8.28 | 0.03 | 557.1 | A, B |
| Ballotini 2 | 0.37 | 0.38 | 380–1460 | 0.00 | 0.24 | Very Well Sorted | 0.91 | 0.93 | -0.10 | 3.61 | 0.75 | 773.1 | B, D |

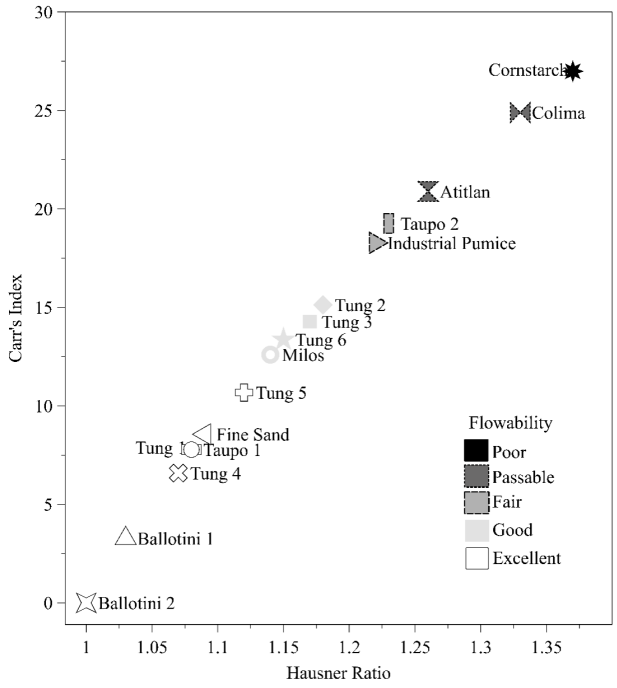


Figure 2: Bulk and tapped bulk density results of dry pyroclastic and analogue materials. Results were used to calculated Hausner ratio and Carr's index to determine flowability. Flowability field values are from Gorle and Chopade [2020]. Materials are in order of particle size mean (Φ). Standard deviation of BTD, uncertainty and error can be found in Supplementary Material B.

### 2.3 Experimental procedure

Bulk and Tapped Density (BTD) measurements were completed to assess the mass and volume relationships of granular material, both in their initial and compacted states [Amidon et al. 2017]. Calculating the material bulk density involved pouring 100 g of the material into a 250 mL cylinder. The initial unsettled volume $V_0$ was measured, and bulk density $\rho_b$ calculated as:

$$\rho_b = \frac{m}{V_0}, \tag{3}$$

where $m$ is mass (g). The cylinder was then tapped at 150 taps/min. The cylinder volume was measured every minute until a stable, levelled reading was completed and tapped density ($\rho_t$) was calculated using (Supplementary Material B):

$$\rho_t = \frac{m}{V_f}, \tag{4}$$

where $V_f$ is the final tapped volume [Moondra et al. 2018].

These experiments were repeated with the addition of water (0–5 wt.%). The bulk and tapped densities were then calculated to see the effect of adding water. This enabled the calculation of the Carr's Index (CI; Equation 5) and Hausner Ratio (HR; Equation 6), which are important parameters for understanding the flowability behaviours of a material (i.e. how easily a material can flow or move):

$$\mathrm{CI} = 100\left(\frac{\rho_t - \rho_b}{\rho_t}\right), \tag{5}$$

$$\mathrm{HR} = \frac{\rho_t}{\rho_B}. \tag{6}$$

Carr's index evaluates a material's strength and compressibility [Moondra et al. 2018]. The Hausner ratio assesses the packing efficiency of the material and its susceptibility to compact under external forces [Yu and Hall 1994; Abdullah and Geldart 1999]. For example, a low HR signifies good flowability behaviours. BTD experiments were conducted for a representative subset of the entire suite of experiments.

Static, and dynamic angle of repose (SAoR and DAoR, respectively) experiments were completed to assess the angle of internal friction and flowability of the material [Beakawi Al-Hashemi and Baghabra Al-Amoudi 2018].

When a granular material is released freely onto a surface, the particles will arrange themselves to form a natural slope, where the maximum slope before collapse is called the static "angle of repose". The angle of repose has been explored in granular science to investigate the physical and mechanical properties, such as the friction coefficient, shear strength and the flowability of granular material [Zhou et al. 2002; Beakawi Al-Hashemi and Baghabra Al-Amoudi 2018; Dai et al. 2022]. In this work, the static and dynamic angle of repose (SAoR and DAoR, respectively) were completed to explore the properties of the bulk behaviour of the particles with the addition of moisture.

For the SAoR experiments, 100 g of each sample was released from a funnel held 35 mm above a circular platform. The cone height was then measured, and the SAoR calculated using:

$$\mathrm{SAoR} = \arctan\left(\frac{2h}{D}\right), \tag{7}$$

where $h$ is the height of the pile formed and $D$ = 85 mm is the base diameter of the platform .

The DAoR experiments were completed by using 100 g of material in a rotating drum. Material was rotated and recorded, and the critical angles were measured using `ImageJ` software [Schneider et al. 2012]. SAoR experiments were repeated three times and a subset of DAoR experiments were run to demonstrate reproducibility (Supplementary Material B).

Finally, fluidisation experiments investigated the fluidisation behaviours and states of each material at varying moisture contents. This adopted the use of a rectangular, near 2D fluidisation chamber with a porous base [Gilbertson et al. 2020; Walding et al. 2023]. Samples of 200 g were placed into the chamber and levelled. A manometer then recorded basal pore pressure changes throughout the experiment. Compressed dry, unheated air was then incrementally passed through the porous base into the chamber and at the points of minimum fluidisation state (i.e. bubbling, channelling, etc.). The tests were run until either a stable fluidisation state was achieved (bubbling or channelling), excessive winnowing of material occurred or where large pressure was reached without any

resulting gas escape structures being formed. Experiments increased the gas flow rate from 0 to 5 cm $s^{-1}$ for a period of 0 min 31 s to 3 min 28 s. The short experimental time aided in limiting the effects of material drying. Given time constraints, we decided to focus on completing a range of fluidisation experiments, rather than repeats of fewer experiments.

### 2.4 Statistical analysis

The experiments presented here explore a wide array of variables. We assess the correlation between the different variables by using Spearman's rank correlation coefficient ($r_s$). The $r_s$ is statistically useful in identifying trends in large data sets and evaluates the monotonic relationship between two independent variables [Gauthier 2001]. From this, the confidence interval can be calculated to better constrain relationship correlations for the use of principal component analysis. A principal component analysis (PCA) is used on all samples to summarize the correlated variables as highlighted using the $r_s$. Data analysis has been completed using the statistical softwares `Microsoft Excel`, `RStudio` (Version 4.3.2, 2023) and the R packages `FactoMineR` [Lê et al. 2008], `factoextra` [Kassambara and Mundt 2016] and `ggplot2` [Wickham 2009].

### 2.5 Limitations

In nature, pyroclastic materials are more polydisperse than the materials used within these experiments. Their natural variation shows a vast distribution of size, density, shape, composition, and temperature than the parameter space explored in this work. The limitations on particle size (<2000 µm) reflects the limitations of equipment size used in the experiments, such as scaling limits of the fluidisation chamber. Future work encompassing a wider size range could overcome this by using larger fluidisation chamber equipment. At high moisture percentages, the materials used in the DAoR experiments begin to clump, stick and slide to the wall of the drum. Therefore, some DAoR values have been excluded from the results.

## 3 Results I: Behaviour of material in dry conditions

### 3.1 Particle size analysis

The pyroclastic materials used in these experiments (Figure 1) have particle size distributions ranging from 2.5 to 2000 µm and the analogue materials (Figure 1) have a particle size distribution from 2 to 1460 µm. Based on the logarithmic particle mean (Table 4) all materials are expected to exhibit fluidisation behaviours typically associated with Groups A and B in Geldart's classification.

### 3.2 Bulk and tapped densities

In dry (0 wt.%) conditions, the finest materials (cornstarch, Colima, Atitlán and Taupō 2) display poor and very poor flowability properties as defined by their HR and CI values (Figure 2).

These correlate with the exceptionally high fines content of these materials (>52 %). The remaining materials all exhibit fair to excellent flowability, which is influenced by both fines content (<52 %) and high sorting values (Table 4; Supplementary Material B).

### 3.3 Angle of repose

At 0 wt.% moisture, the SAoR of the pyroclastic samples range from 28° (Milos) to 43° (Taupō 1, Colima), and the analogue materials from 18° (ballotini 1) to 38° (cornstarch;Supplementary Material B). Comparing these results against the materials properties in Table 4, demonstrate that the increase in SAoR correlates to size, shape, and sorting (Figure 3). The DAoR ranges from 39° (Tung 5 and 6) to 61° (Atitlán) for pyroclastic samples and from 32° (ballotini 1 and 2) to 59° (cornstarch) for the analogue materials. An increase in particle size median results in an increase in both SAoR and DAoR (Figure 3A). Fines content also plays a dominant role on angle values. As fines contents increase, SAoR and DAoR increase until ~52% fines where we see a divergence and larger gap between DAoR and SAoR values (Figure 3B). With an increase in $D_{32} \cdot \mathrm{SPHT}$, we see lower SAoR and DAoR values (Figure 3E and 3F). Finally, sphericity and symmetry controls on SAoR and DAoR are demonstrated in Figure 3C and 3D, where a decrease in SAoR and DAoR correlates with increasing sphericity and symmetry. This is particularly evident for ballotini 1, which has the highest sphericity (0.90, 0.91) and symmetry values (0.93, 0.93).

### 3.4 Fluidisation

Results from the fluidisation experiments were investigated via sidewall video analysis of the fluidisation chamber. We used ballotini to characterise the frictional properties against the side wall (Perspex) by completing tilt experiments (experimental set-up from Lowes and Perry [1965]). This allowed us to calculate the dry wall friction angle, which showed a value of 21.5° (standard deviation of 2.4°). Note that this value is likely to change with the addition of moisture and during fluidisation of material but has not been further explored in these results.

Observations of gas escape structures (e.g. bubbling, channelling) were taken and gas velocity was recorded from the base of the chamber. Fluidisation behaviours are categorized into bubbling ($U_{mb}$), channelling ($U_{mc}$), explosive channelling ($U_{mx}$) and cracking behaviours ($U_{mcr}$) following Walding et al. [2023] (Figure 4). In addition, a new feature is identified in this paper and named "diffusive cracking" ($U_{mdc}$, Figure 4F, Supplementary Material C). Diffusive cracking is defined here as small cracks that can move in-between packages of material and are not fixed (in comparison to cracking, where wet material forms large cracks which only move with increased drying of the material). The individual packages in diffusive cracking can be fluidized, or as gas velocities increase, the packages of material can fracture into smaller packages aiding bubbling and channelling before once again settling into a package and repeating behaviours as mentioned above (Figure 4F).

#### 3.4.1 *Pyroclastic materials*

At 0 wt.% moisture, the pyroclastic samples exhibit bubbling, diffusive cracking, channelling, and explosive channelling. Milos, Taupō 1 and Taupō 2 display channelling of the coarser

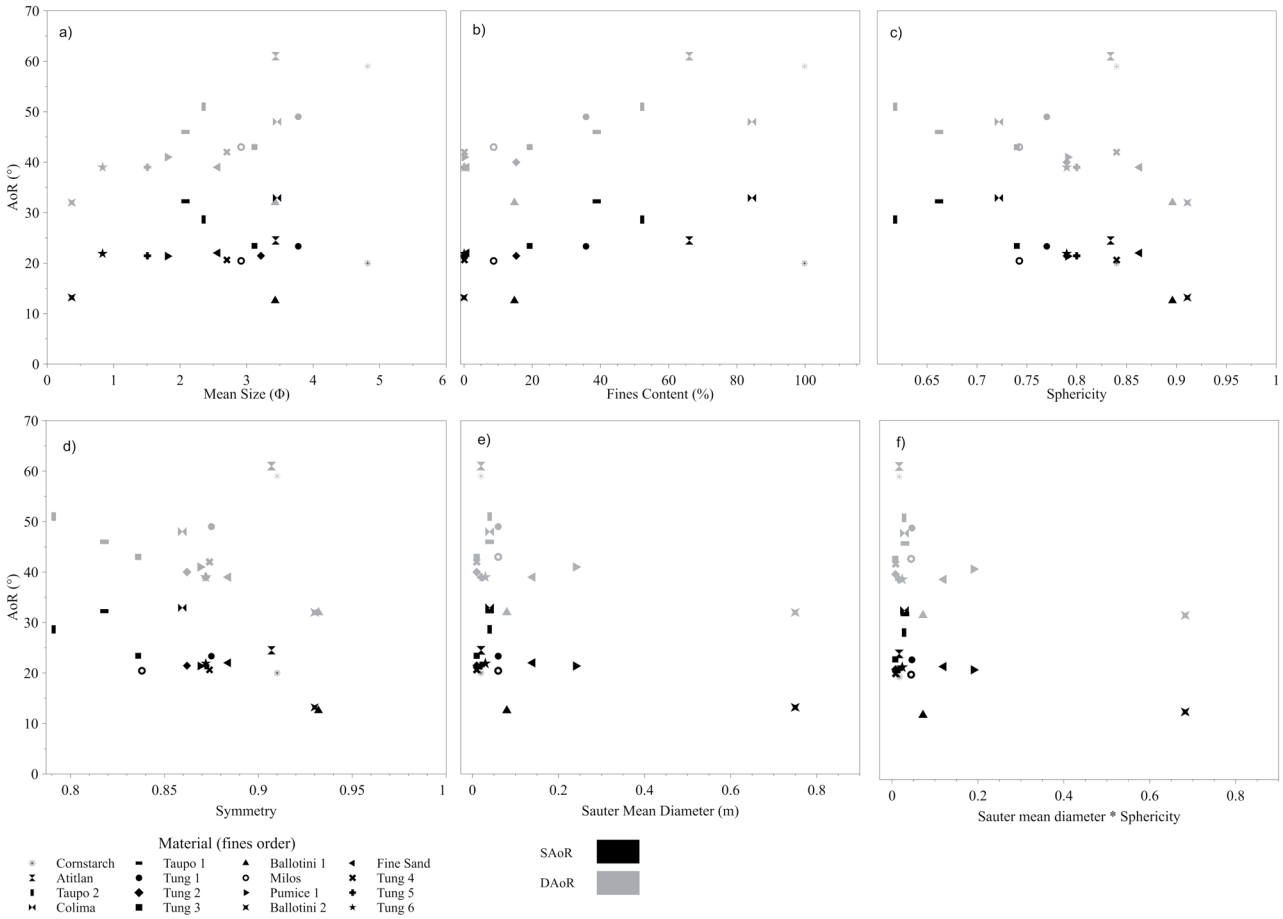


Figure 3: Comparison of particle [A] methods of moments logarithmic mean size, [B] fines content, [C] sphericity, [D] symmetry, [E] Sauter mean diameter and [F] Sauter mean × sphericity ($D_{32} \cdot \mathrm{SPHT}$) against SAoR and DAoR values of pyroclastic and analogue materials. Materials are listed in order of fines content (%). Standard deviation, error and uncertainty are shown in Supplementary Material B.

material in the lower deposit and bubbling in the upper deposit ($U_{mb}$: Milos, 0.28; Taupō 1, 0.21; Taupō 2, 0.14 cm s$^{-1}$). However, Colima and Taupō 1 show small amounts of diffusive cracking with no significant change in pressure observed (Figure 4F). At 0 wt.% moisture, both the diffusive cracking ($U_{mdc}$: Taupō 1, 0.069; Colima, 0.069 cm/s) and explosive channelling ($U_{mx}$: Atitlán, 0.069; Colima, 0.208 cm/s) agitate the material and improve heterogeneous bubbling and channelling throughout the whole of the deposit (Figure 4A–4F).

The variations in fluidisation behaviours of Atitlán, Colima and Taupō 1 can be attributed to their high fines content (38–84%; Table 4). Fluidisation and $U_{mb}$ values are significantly lower in material with a higher proportion of fines. These are indicative of Geldart Group C behaviours. Taupō 2 also displays a high percentage of fines (52%) but does not display cracking or explosive channelling at 0 wt.% moisture. This corresponds to the behaviours seen in the Tungurahua and Milos samples, where sorting is moderate to well sorted.

### 3.4.2 *Analogue materials*

Fluidisation experiments with the cornstarch were not attempted due to its tendency to disperse into the air. At 0 wt.% moisture, all the other analogue samples tested display bubbling of the deposit (Geldart Group B; Figure 4). In the finer material (ballotini 1), bubbles are small and spherical and form throughout the whole of the deposit ($U_{mb}$ = 0.056 cm s$^{-1}$). Ballotini 2 and fine sand are overall coarser and denser materials, so sluggish bubbling is limited to the upper portion of the deposit ($U_{mb}$: ballotini 2, 2.08; fine sand, 0.417 cm s$^{-1}$). Finally, the industrial pumice has a larger size range than the others and exhibits channelling of the lower coarser material and bubbling ($U_{mb}$ = 0.382 cm s$^{-1}$) of the upper finer material (Figure 5). The good fluidisation behaviours of these materials can be attributed to the low fines content (0.00–14.78%) and moderate to well sorting values (Table 4). Furthermore, the fluidisation behaviours of the analogue material at 0 wt.% moisture all exhibit Geldart Groups A, B and C characteristics [Geldart 1973].

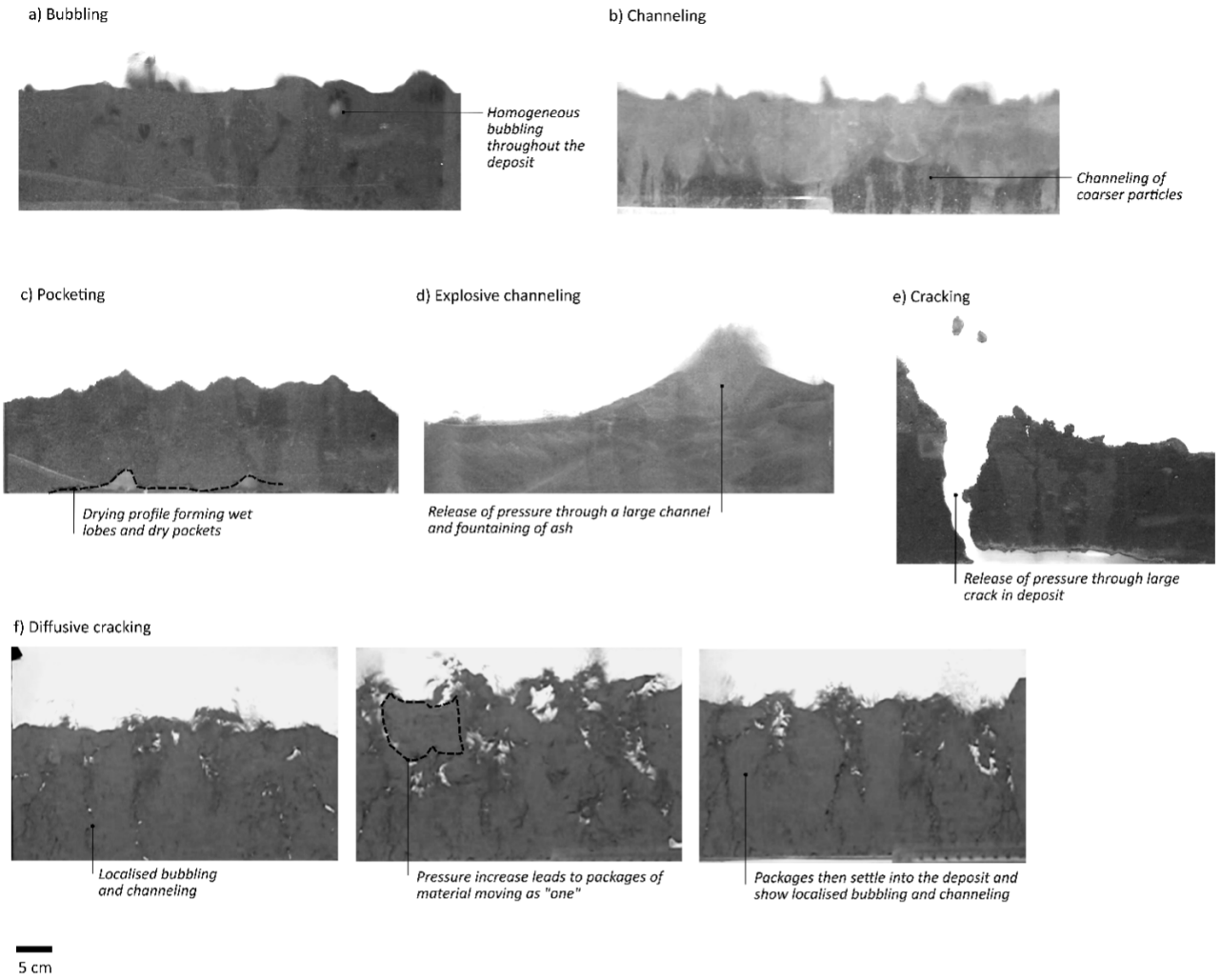


Figure 4: Images demonstrating the key behaviours described in these experiments showing [A] bubbling, [B] channelling, [C] pocketing, [D] explosive channelling, [E] cracking [from Walding et al. 2023], and [F] diffusive cracking features seen in the present fluidisation experiments.

## 4 Results II: behaviour of material in wet conditions

### 4.1 Bulk and tapped densities

With increasing moisture contents (0–5 wt.%), bulk and tapped densities overall decrease rapidly with an increase from 0 to 0.5 wt.% moisture and then steadily from 0.5 to 5 wt.% moisture (Supplementary Material B). However, this is not the case for ballotini 1 and 2. From 0–0.5 wt.% moisture, ballotini 2 increases in tapped density before levelling out. The tapped density for ballotini 1 shows a decrease in density from 0–1 wt.% moisture before increasing in tapped density from 1–5 wt.% moisture. Both particles are highly spherical and hydrophobic, therefore added water may form capillary bridges between the particles. It is thought that with increasing water, lubrication is increased, allowing for the particles to display overall better packing.

The Hausner Ratio and Carr's Index calculations can be used to assess how moisture effects the flowability of a material (Supplementary Material B). The largest change seen in both CI and HR from 0–5 wt.% moisture are Tung 4 samples and the lowest change was seen in Tung 6. This is thought to be due to the high sorting and small size range of Tung 4 and the high size mean of Tung 6 (Table 4). The CI and HR results show that increasing moisture (0.5–5.0 wt.%) has a negative effect on the flow property of the material (i.e. showing poorer and more difficult flowability; Figure 6). However, this is not the case for Tung 6 which decreases in CI and HR. This is thought to be due to water induced lubrication and better packing of material.

### 4.2 Angle of repose

An increase in moisture from 0 to 5 wt.% results in an increase in SAoR and DAoR values for pyroclastic and analogue materials and therefore a decrease in flowability (Supplemen-

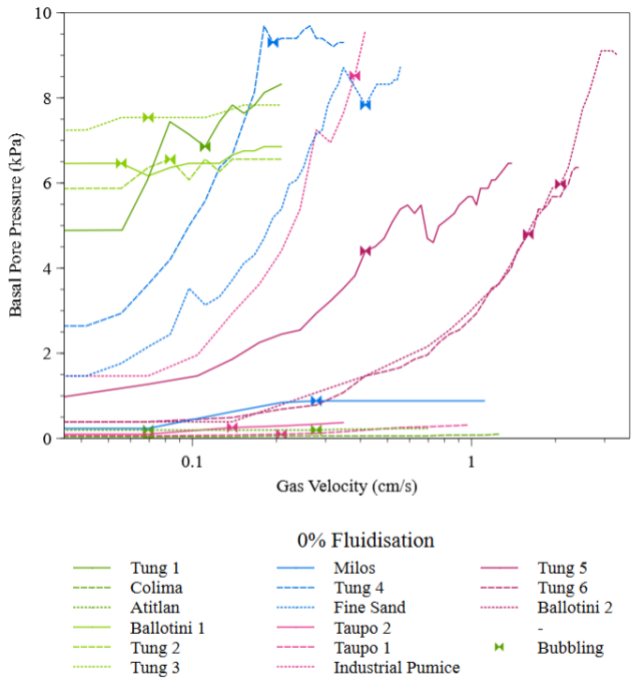


Figure 5: Fluidisation profiles of pyroclastic and synthetic materials at 0 wt.% moisture. Tung 1–6 values obtained from Walding et al. [2023]. Materials are in order of particle size mean (Φ).

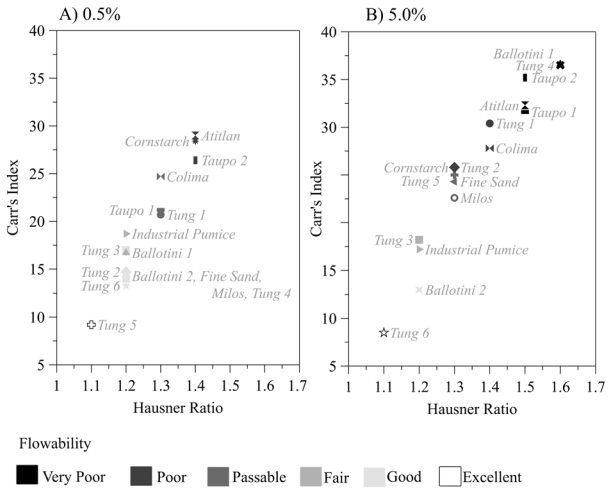


Figure 6: Changes in Hausner Ratio and Carr's Index as a function of water addition to the material for [A] 0.5 wt.% and [B] 5 wt.%. Flowability field values are from Gorle and Chopade [2020]. Materials are in particle size mean (Φ) from finest (cornstarch) to coarsest (ballotini 2). Standard deviation, error and uncertainty of BTD can be found in Supplementary Material B.

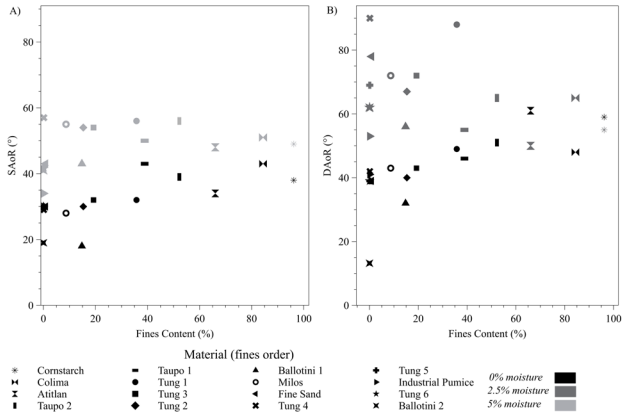


Figure 7: [A] SAoR at 0 and 5 wt.% moisture and [B] DAoR at 0 and 2.5 wt.% moisture of pyroclastic and analogue materials and fine content (%). Materials are listed vertically are in order of fines content (%) from cornstarch to Tung 6. Standard deviation, error and uncertainty are in Supplementary Material B.

tary Material B). Further detailed analysis of Tungurahua 1–6 samples can be found in Walding et al. [2023].

#### 4.2.1 *Pyroclastic materials*

Overall, the highest SAoR change (>29°) from 0 to 5 wt.% moisture are seen in Tung 1, Tung 2, Tung 3, Milos, Tung 4 and Tung 5. From 0 to 1 wt.% moisture, Tung 2, Tung 3, Tung 4 and Tung 5 show a rapid increase in SAoR which then increases at a lower rate from 1 to 5 wt.% moisture (Supplementary Material B). In some materials (Tung 2, Tung 3) we see a decrease in SAoR value at 5 wt.% moisture. Taupō 2, Colima, and Atitlán show the smallest change from 0 to 1 wt.% and some of the largest from 1 to 5 wt.% moisture. The lowest overall SAoR change (8°) from 0 to 5 wt.% moisture is Colima. For the DAoR experiments, the highest change from 0 to 2.5 wt.% moisture is Tung 1 (39°) and Tung 4 (48°) and the lowest is Atitlán (−11°) (Figure 7).

The overall largest changes are seen in the Tungurahua and Milos samples. These samples span the size range of pyroclastic mean sizes, are all moderately to well sorted (0.252–0.868) and show similar sphericity values (0.74–0.84) (Table 4). These samples also all display the lowest fines content ranging from 0.04% (Tung 6) to 36% (Tung 1) (Figure 7). Conversely, the lowest overall changes as seen in Colima, Atitlán, Taupō 1 and Taupō~2 which have a broad size mean, are moderately to poorly sorted (0.98–1.50) and sphericity values of 0.70–0.83. Notably, these samples display the highest fines content which ranges from 39% (Taupō 1) to 84% (Colima) (Figure 7).

#### 4.2.2 *Analogue materials*

Values of SAoR increase with increasing moisture from 0 to 5 wt.%. From 0 to 1 wt.% moisture, ballotini 1 and ballotini 2 show a rapid increase in SAoR (Figure 7). Cornstarch, fine sand and industrial pumice all show a more gradual increase. From 1 to 5 wt.% moisture the SAoR values become steadier and ballotini 1, fine sand and ballotini 2 all show the same or lower values than their 1 wt.% moisture SAoR results. The largest changes can be seen in the ballotini 1 and ballotini 2

samples. These samples are both moderately well to very well sorted (0.62–0.24) and have high sphericity values of 0.90 and 0.91 (Table 4, Figure 7). The lowest overall change is cornstarch (11°), which displays the largest size range, sorting value (0.989) and lowest sphericity value (0.79).

The DAoR experiments show a similar pattern, where from 0 to 2.5 wt.% moisture there is an increase of DAoR in ballotini 1 (24°), fine sand (39°), industrial pumice (12°) and ballotini 2 (30°). However, the cornstarch shows a decrease of −4° with increasing moisture from 0 to 2.5 wt.%. This is due to the high percentage of fines in cornstarch (96.1%) compared to the other samples (Table 4).

### 4.3 Fluidisation

The results presented correspond to the observed fluidisation behaviours of both pyroclastic materials (Atitlán, Colima, Milos, Taupō 1 and Taupō 2) and analogue materials (ballotini 1, ballotini 2, fine sand, industrial pumice) utilised in these experiments across water addition of 0.50, 1.00, 2.50 and 5.00 wt.%. A detailed review of the fluidisation behaviours of Tungurahua 1–6 samples can be found in Walding et al. [2023] and Supplementary Material D. Overall, results show that with increasing water content, a higher gas velocity is required to fluidise the material. A Geldart Group has been assigned to the fluidisation behaviours observed throughout the experiments [Geldart 1973; Cocco and Chew 2023].

#### 4.3.1 *Pyroclastic materials*

At 0.50 wt.% moisture (Figure 8A, 8F), Colima ($U_{mb}$ = 0.139 cm s$^{-1}$) and Taupō 2 ($U_{mb}$ = 0.069 cm s$^{-1}$) display bubbling towards the top of the deposit and diffusive cracking at the base (Geldart Groups A and C). When the cracking ruptures, the overlying material is agitated and bubbles with the rest of the deposit before settling to the base of the deposit. Atitlán ($U_{mb}$ = 0.069 cm s$^{-1}$) and Taupō 1 ($U_{mb}$ = 0.069 cm s$^{-1}$) (Figure 8B, 8G) show bubbling of the upper and channelling of the lower deposit (Geldart Groups A, B and C). Milos (Figure 8D) forms pockets of bubbling ($U_{mb}$ = 0.972 cm s$^{-1}$) at the base of the material, which increase in size throughout the experiment (Geldart Group B).

At 1.00 wt.% moisture (Figure 8B), Atitlán shows bubbling throughout the upper portion of the deposit ($U_{mb}$ = 0.069 cm s$^{-1}$) and channelling in the lower portion (Geldart Group B). Colima, Taupō 1 and Taupō 2 (Figure 8A, 8F, 8G) show diffusive cracking in the deposit and some bubbling at $U_{mdc}$ of 0.556, 0.347 and 0.208 cm s$^{-1}$, respectively (Geldart Groups B and C). At higher gas velocities, explosive channelling happens multiple times throughout the deposit, but does not release significant amounts of pressure from the base.

At 2.50 wt.% moisture (Figure 8B), Atitlán shows bubbling throughout the upper portion of the deposit ($U_{mb}$ = 0.069 cm s$^{-1}$) and channelling in the lower (Groups A and C). Explosive channelling occurs at 0.972 cm s$^{-1}$ for Colima (Figure 8A) followed by a large pocket forming with bubbling and drying of material (Geldart Groups C and A; $U_{mb}$ = 1.11 cm s$^{-1}$). Taupō 1 and Taupō 2 (Figure 8F, 8G) display explosive channelling and cracking (Geldart Group C), but with no observed gas release. Bubbling observed in Taupō 1 ($U_{mb}$ = 1.25 cm s$^{-1}$) is sluggish. Small pocketing occurs at the base of the Milos (Figure 8D) deposit, with no observed bubbling (Geldart Group C). Slow drying continues until the end of the experiment.

Finally, at 5.00 wt.% moisture (Figure 8B), Atitlán again shows similar behaviours as described previously and bubbles at 0.069 cm s$^{-1}$ (Geldart Group A). Milos (Figure 8D) shows cracking at 3.19 cm s$^{-1}$ and explosive channelling at 4.17 cm s$^{-1}$ (Geldart Group C). Taupō 1 (Figure 8F) forms a large pocket at the base of the deposit, slight cracking (1.39 cm s$^{-1}$) and explosive channelling at 1.53 cm s$^{-1}$ (Geldart Group C). Finally, Taupō 2 (Figure 8G) bubbles in a sluggish way in the upper deposit ($U_{mb}$ = 0.069 cm s$^{-1}$) and displays channelling in the lower deposit. With increasing gas velocity, cracks begin to form and breakaway from each other in "blocks" which rise and fall (Geldart Group C).

Compared to the Tungurahua 1–6 samples (Supplementary Material D), Atitlán, Colima, Taupō 1 and Taupō 2 exhibit "higher moisture" fluidisation behaviours (Group C: i.e. cracking and explosive channelling) at significantly lower moisture levels. These materials also display significantly higher fines content (%) than any other samples (Table 4). This may explain why we see more sluggish bubbling behaviour and diffuse cracking happening at a lower moisture content.

#### 4.3.2 *Analogue materials*

At 0.50 wt.% moisture (Figure 8), no gas escape structures are observed in ballotini 1 and ballotini 2. Fine sand (Figure 8E) and industrial pumice (Figure 8H) both display bubbling ($U_{mb}$ = 0.292 and 0.458 cm s$^{-1}$, respectively) in the upper deposit and channelling of the lower (Geldart Groups A, B and C). At higher gas velocities, explosive channelling (0.514 cm s$^{-1}$) occurs in the fine sand but there is no significant change in pressure.

At 1.00 wt.% moisture, no gas escape was observed for ballotini 1 and ballotini 2 (Figure 8C, 8I). Once material was dried by the fluidising gas, the ballotini deposit had stuck together as a "fused" package and had to be manually broken apart. No further fluidisation experiments were undertaken on the ballotini samples. Both the fine sand and industrial pumice exhibited pocketing and bubbling of dry material at 0.2778 and 0.5694 cm s$^{-1}$ (Geldart Groups A, B and C). At higher gas velocities, explosive channelling was observed in the industrial pumice. Explosive channelling at 1.069 cm s$^{-1}$ released 0.33 kPa. Due to time constraints, fluidisation of industrial pumice at 2.5 and 5 wt.% were not completed.

At 2.50 wt.% moisture, fine sand (Figure 8E) forms bubbling pockets at 0.69 cm s$^{-1}$ and explosive channelling at 1.81 cm s$^{-1}$ (releasing 0.69 kPa). Finally, at 5.00 wt.% moisture (Figure 5B) fine sand shows pocketing and subsequent bubbling of the material ($U_{mb}$ = 1.39 cm s$^{-1}$) (Geldart Groups C and A).

## 5 Discussion

In this discussion, we identify the key controls that influence the behaviours of pyroclastic material with increasing moisture content. We then discuss material recommendations for

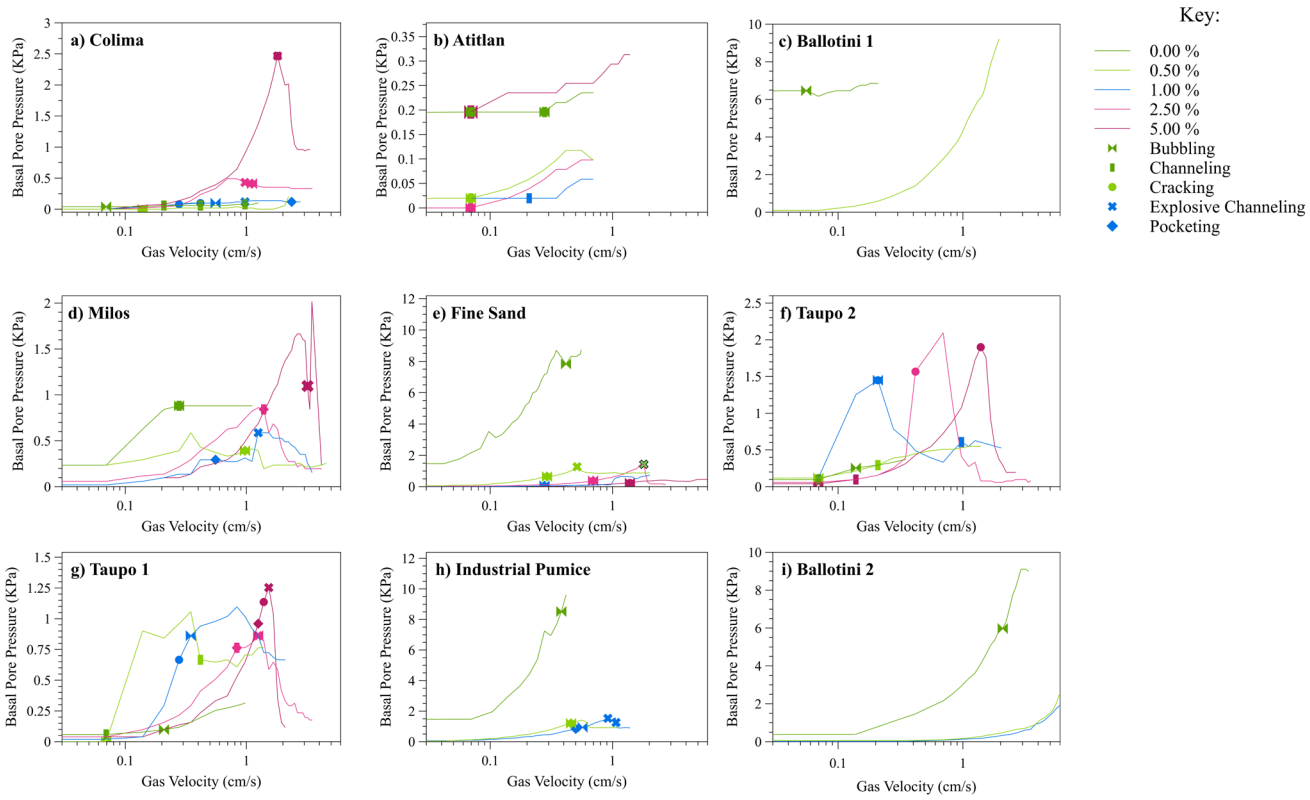


Figure 8: Fluidisation behaviours of pyroclastic and analogue materials at 0, 0.5, 1, 2.50 and 5 wt.% moisture addition [A] Colima, [B] Atitlán, [C] Ballotini 1, [D] Milos [E] Fine Sand, [F] Taupō 2, [G] Taupō 1, [H] Industrial Pumice [I] Ballotini 2. Symbols show fluidisation behaviours of material. Data is presented in material mean size order. Fluidisation results from Tung 1–6 are in Supplementary Material D.

use in experimental modelling in dry and wet conditions in a flow and substrate.

### 5.1 Controls on behaviour of pyroclastic material

To better constrain the controls on material behaviours in dry and wet conditions, we conducted principal component analysis (PCA) on SAoR and DAoR results and material characteristics (e.g. symmetry, sphericity, particle size mean, sorting, Sauter mean, geometric mean and fines content).

The results from the PCA analysis (Figure 9; Supplementary Material E) show that SAoR and DAoR values at 0 wt.% moisture correlate to mean, fines content, sorting, HR and CI. However, as we increase moisture from 0 to 0.50 wt.% the results become more positively correlated with sphericity, symmetry and Sauter mean and therefore more negatively with sorting and fines content. A further increase in moisture from 0.50 to 2.5 wt.% shows no correlation to any of the aforementioned variables.

These results are interpreted as reflecting the transition of the material from a non-capillary to a capillary state with the introduction of water. In the capillary state [Kim and Hwang 2003; Kim and Sture 2008] particles become semi-supported by capillary bonds. With no moisture, the SAoR and DAoR is dominated by material characteristics (fines and sorting) as there are no inter-capillary bonds present. At low moisture addition, the control becomes more correlated to physical particle characteristics (sphericity and symmetry). Finally, at the highest moisture values, we infer a transition due to changes in capillary bonds forming in interparticulate spaces, and thus, behaviours are less controlled by material parameters (i.e. fines content, shape, etc.).

#### 5.1.1 *The importance of the proportion of fines content*

The presence of fines in a material influences its behaviour in both static and dynamic conditions, as well as in wet and dry environments, as demonstrated in the BTD (Figure 2, 6; Supplementary Material B), SAoR (Figure 3, 7; Supplementary Material B), DAoR (Figure 3, 7; Supplementary Material B), fluidisation (Figure 5, 8A–8I) tests and PCA results (Figure 9). At 0 wt.% moisture, the angle of repose (both SAoR and DAoR) increases with mean size, sphericity, symmetry, Sauter mean and proportion of fines content (up to ~66%). Note that the DAoR results are significantly higher than the SAoR results, this is attributed to boundary friction of the drum [Dury et al. 1998]. At 84% fines content, there is a clear divergence between SAoR (decreasing) and DAoR (increasing) values (Figure 3B). Interestingly, at very high fines contents, pyroclastic material shows a decrease in flowability in a dynamic environment and an increase in flowability in a static environment (Figure 3B, 7). This may indirectly influence the mechanical properties of a material, such as the friction coefficient and cohesion-related shear strength [Beakawi Al-Hashemi and

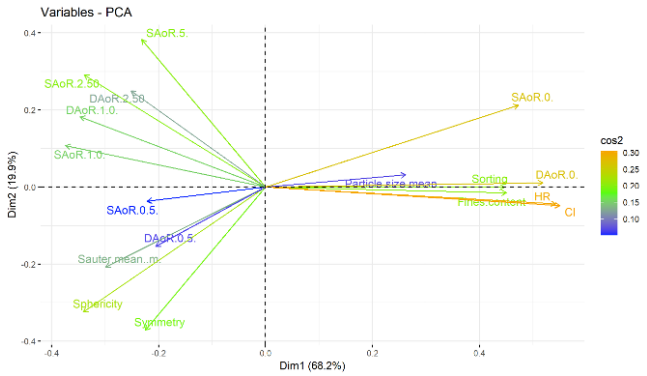


Figure 9: Loading plot from PCA analysis [Lê et al. 2008; Kassambara and Mundt 2016; Team 2023]. Dim1 and Dim2 are the principal components and show percentages. Each variable used in the data set is showed as a vector. The direction of the vector indicates the correlation between the variable and the principal component, while the length of the vector represents the magnitude of the correlation (cos2). Vectors that group together or point in similar directions may indicate similarities or underlying relationships.

Baghabra Al-Amoudi 2018]. For example, a material that has greater than 30% volume of fines results in the stress forces being dominated by the fines fraction [Li et al. 2020; Breard et al. 2023].

In dry conditions, material with a low fines content can be expected to behave based on its physical particle characteristics such as size, sphericity, and symmetry [Abdullah and Geldart 1999]. With increasing sphericity of a particle, the angle of repose will decrease; and vice versa, with decreasing sphericity of a particle (i.e. increasing angularity), the angle of repose will increase [Beakawi Al-Hashemi and Baghabra Al-Amoudi 2018]. This is due to interparticle contacts, where angular particles increase jamming and interlocking connections [Beakawi Al-Hashemi and Baghabra Al-Amoudi 2018]. Our results somewhat agree with these observations as seen through the sphericity and symmetry values increasing in Figure 3C and 1D.

The addition of moisture to material with high fines content leads to a decrease in both SAoR (cornstarch, Colima, Atitlán, Taupō 2; Figure 7A) and DAoR (cornstarch Atitlán and Colima; Figure 7B) values. This may be due to friction between particles due to particle morphology characteristics and moisture-induced clumping of material. The fines material is more likely to form interlocking "clumps" of material in dry conditions or moisture-induced clumps when wet. In turn, both instances of clumping will increase the size of the material to form more spherical clumps, which are more likely to have greater translational and rotational velocities [Chen et al. 2019]. Similarly, the presence of fines significantly increases the material surface area [Figure 8E, 8F; Huang et al. 2009] and the surface tension of free moisture cannot mix well in the fines-dominated mixture. This may result in the formation of liquid bridges which reduce the contact friction, resulting in a decrease of SAoR and DAoR values.

Bulk behaviour can significantly change with fines content [Beakawi Al-Hashemi and Baghabra Al-Amoudi 2018]. An increase in fines creates more interparticle contact points, which in turn can increase the packing of material [Breard et al. 2023]. This is demonstrated in the BTD experiments where loose and tapped bulk densities increase with fines content and size (e.g. cornstarch, Colima, Atitlán; Supplementary Material B). This leads to better packing of material and thus poorer flowability. This also corresponds to what we observe in the DAoR experiments where an increase in fines content and a decrease in size results in higher DAoR values, and therefore a poorer flowability value (Figure 2). These results highlight a clear relationship between fines content, particle size, loose/tapped behaviour and flowability.

#### 5.1.2 *Age, composition and environment effects*

Age, composition, and environment will all play a role in the decay or alteration of material [Nagasawa 1978]. Furthermore, post-deposition hydrothermal alteration over time may cause the alteration and decay of minerals into clay [Mirabella et al. 2005]. Increasing clay content may result in changes in physical material properties (i.e. increase in cohesion, fines content, density, etc.). We examined our results against composition and age of material to rule out any effect of age or composition on our results.

Our samples range from felsic (Taupō 1, 2 and Atitlán), intermediate (Milos) and mafic (Colima and Tung 1–6) in composition [Table 2; Wilson 1984; Kelfoun et al. 2009; Eychenne et al. 2012; Douillet et al. 2013; Hall et al. 2013; Zhou et al. 2021]. The degree of magmatic evolution does not appear to be correlated with the changes in cohesive behaviour with increasing moisture. In this study, we have found no correlation between ages of samples to cohesive behaviours (from the SAoR and DAoR experiments). For example, the Tungurahua (Tung 1–6) samples from 2006 showed significantly higher SAoR difference from 0 to 5 wt.% moisture (22–29° difference between 0 and 5 wt.% SAoR) in comparison to the more recent 2015 Colima samples (8° difference between 0 and 5 wt.% moisture SAoR). The oldest Taupō samples (235 AD) show a change of 17° (Taupō 1) and 18° SAoR (Taupō 2) from 0 – 5 wt.% moisture.

### 5.2 Implications for PDCs and their Deposits

Static and dynamic friction coefficient and shear strength, as determined by the SAoR and DAoR values will play a critical role at different stages within a PDC system. For example, static friction coefficient may play an important role in the initial movement, remobilisation and entrainment of sediment from an overriding PDC. Once material is moving, dynamic friction will be the dominant force. However, in the case of the DAoR method used in these experiments, the angle of repose is high which is thought to be due to boundary friction of the drum.

#### 5.2.1 *Implications for deposits*

In Walding et al. [2023] three types of gas escape structures were observed, dependent on moisture content. Type 1 (0–0.25 wt.% moisture) showed bubbling and channelling of ma-

terial and relatively "good" fluidisation behaviours. Type 2 (0.50–5.00 wt.% moisture) resulted in bubbling, channelling, pocketing, a drying profile and explosive channelling. Type 3 (7.50 and 10 wt.% moisture) showed a bubbling drying profile, pocketing and cracking of the deposit (Figure 4A–4D). These results showed that fluidisation and gas escape may be stalled or stopped by the presence of moisture (from 0.50 wt.%).

In this study, we observe the same gas escape structures as Walding et al. [2023], but sometimes at significantly lower moisture contents. Additionally, we describe a new behaviour, "diffusive cracking" (Figure 4E; Supplementary Material C). The present study expands on the types of behaviour of gas escape shown in Walding et al. [2023] and demonstrates that gas escape structures are highly variable with differing material characteristics, their geomechanical properties and moisture content.

Material behaviours differed greatly with varying presence of fines. At a high fines percentage (>38%) fluidisation behaviours behave more like the "high moisture" structures (i.e. explosive channelling, cracking) seen in Walding et al. [2023]. This is due to the larger influence from Group C Geldart Group particles [Geldart 1973]. In dry conditions, Group C particles are dominated by interparticle forces and are known to demonstrate poor fluidisation behaviours of spouting, slugging, and channelling [Leturia et al. 2014]. Materials moved through the different fluidisation stages described by Walding et al. [2023] with increasing moisture. However, the Atitlán material which comprises of 66% fines showed no significant changes in fluidisation behaviour with increasing moisture. This may be due to having a large surface area, or the presence of $H_2O$-scavenging minerals. Further study would benefit from investigating the impact of varying chemical composition and $H_2O$ scavenging in more detail.

#### 5.2.2 *Implications for secondary explosions*

We show that secondary explosions may form from the cohesive nature of a dry high fines (%) material as well as with the introduction of moisture, expanding the findings of Walding et al. [2023]. This behaviour is demonstrated in work completed by Gilbertson et al. [2020] where vertical changes in fine and coarse particle sizes resulted in secondary explosions. The cohesive nature of fine material creates an almost impermeable deposit therefore hindering gas release Torres et al. [1996] and Gilbertson et al. [2020] and subsequent pressure increase and release.

#### 5.2.3 *Implications for flow behaviour*

We demonstrate an increase in cohesive behaviour, and resulting shear strength, with increasing fines content and moisture, consistent with the findings of Walding et al. [2023]. However, at high volumes of fines (>84%), 0 wt.% moisture SAoR values decrease, therefore suggesting an increase in flowability. Breard et al. [2023] suggest that fines and packing behaviours can explain the relative long run-out distances of block and ash flows, as an increase in fines increases packing behaviour and elevates pore pressure within the flow. Our results support this finding, where with increasing fines %, flowability increases.

Walding et al. [2023] hypothesised that an increase in fines and moisture influences the cohesive behaviours and therefore, higher moisture contents may reduce flowability and reduce the maximum runout distances of PDCs. However, at the maximum volume of water added (2.5 and 5 wt.%) in these experiments, material with a high fines content >84% showed a decrease in SAoR (cornstarch, Colima, Atitlán and Taupō 2) and DAoR (cornstarch, Colima) values, suggesting an increase in flowability.

The moisture content ranges used in these experiments are not high enough to mobilise the material as a slurry, therefore, the changes in flowability state are not due to the material becoming "laharic" or "saturated". This may have implications for PDCs with a high proportion of fines in moisture influenced environments, such as phreatomagmatic or phreatic events [McPhie et al. 1990]. In this work we only looked at the finer fractions of material, compared to the natural polydisperse nature of PDCs. Future work would benefit from investigating this behaviour at the bulk scale, or whether this behaviour is just indicative of a fine material. Furthermore, the use of a fluidised channel may show these behaviours better.

Our results from the $D_{32}$·SPHT, SAoR and DAoR data (Figure 3E, 3F) show that fines-rich and irregular shaped mixtures will have low permeability, indicating that gas retention and fluidisation may be increased [Breard et al. 2019]. This is also supported by our fluidisation experiments, where finer material shows diffusive cracking (Figure 4F) in comparison to bubbling (Figure 4A, Supplementary Material C), suggesting that increased surface area is influencing frictional drag from the fluidising gas.

### 5.3 Material recommendations for experimental modelling

We have demonstrated that material behaviour is controlled by various properties which may have implications for PDCs and their deposits. Therefore, it is important to choose analogue material carefully, depending on the behaviour experimentalists are aiming to recreate. Here, we compare the material behaviours of pyroclastic samples with a range of analogue materials. We discuss the suitability of those materials for use in experiments conducted under both dry and wet conditions.

#### 5.3.1 *Dry experiments*

*For simulating a flow*

Analogue material is often chosen based on its ability to fluidise in small laboratory experiments [Roche et al. 2010; Rowley et al. 2014; Smith et al. 2018]. In this work we only investigate fluidised flow behaviour rather than free-falling from gravity. The particle size measurements suggest that all material should be able to exhibit good fluidisation behaviours, associated with Groups A and B of Geldart's classification [Geldart 1973]. This is important because, in analogue experiments it is important that the clogging of fine material in hoppers does not occur.

Due to the analogue materials used in these experiments having less polydispersity (e.g. size range, fines content, shape parameters) than the natural, pyroclastic material, it is thought that these will present better flowability and fluidisation results. As the size ranges of our analogue materials span the

size ranges of the pyroclastic material, it is expected that finer particles (i.e. cornstarch) may behave in a similar manner to fine pyroclastic particles (e.g. our Atitlán or Colima sample). This is the same for the coarser material such as Tung 6 against ballotini 2.

For the dry SAoR experiments, cornstarch, fine sand and industrial pumice fall into the range of all the pyroclastic material used (Table 5). In the DAoR experiments, the dry values of analogue material lie in between 39–59° DAoR and for pyroclastic material range from 39 to 61° DAoR. However, both ballotini 1 and ballotini 2 show dramatically lower DAoR values of 13° to 32° for DAoR and therefore, generally do not fit too well when comparing to pyroclastic material in a dynamic testing environment (Table 5).

The results of the fluidisation experiments completed demonstrate that $U_{mf}$ is greater with increasing particle size mean and increasing density (Tung 5, Tung 6, ballotini 2). However, $U_{mf}$ can also increase with mean particle size and with the proportion of fines content within the material. This results in more Group C behaviour [Geldart 1973] of powders, where fluidisation begins to be inhibited by cohesive forces between finer particles. The results from the static (SAoR and BTD) experiments can also be used to calculate the flowability of a material. The results from these static tests correlate well to what is observed in the fluidisation experiments. However, with increasing fines content the projected flowability from the static experiments does not match that of the fluidisation experiments. This is best shown in the behaviours of cornstarch, Atitlán, Taupō 2 and Colima where with increased fines content we see a decrease in SAoR values (Figure 3B). Therefore, for material at high fines concentration it is important that we not only consider the use of SAoR and BTD in determining flowability behaviours, but also how the material will perform in a fluidised environment.

For experiments where matching fluidisation behaviours is important, fine sand, ballotini and cornstarch show the closest match to the range of natural samples used in this study (Table 5). However, it should be noted that although ballotini shows useful fluidisation behaviours in comparison to pyroclastic material, the BTD and SAoR values are considerably lower in a dry environment. This is due to their high sphericity and smoothness, which will reduce contact friction between particles. For future experiments, the combination of different mixtures of these materials could potentially be used to simulate a full dynamic regime (i.e. turbulent to granular).

Although we have been careful to consider a range of pyroclastic options in these experiments, their natural variability means that different experiments may benefit from using different types of material. It should be noted that the practical considerations of using ballotini (i.e. being readily available, easy to characterize, does not deform, does not break) as well as its good fluidisation behaviour [Roche et al. 2004; Roche 2012; Rowley et al. 2014; Smith et al. 2018] are of importance. Therefore, different experiments (i.e. such as fluidisation-based experiments) will benefit from different materials (i.e. good flowability results of ballotini). In the case of SAoR experiments, ballotini shows approximately half the values of the pyroclastic material. Therefore, descriptions remain qualitative when exploring bedforms of flow deposits using ballotini. A more quantitative bedform analysis will require materials with frictional behaviours similar to natural pyroclastic sediments.

*For use as a substrate for flume experiments*

The strength or resistance of a material can be determined by its interparticulate forces (i.e. capillary, van der walls or electrostatic). Their influence can cause fundamental material properties to change, resulting in variations in material strength [Pierrat and Caram 1997; Kim and Sture 2008; LaMarche et al. 2016; Chen et al. 2021]. This can determine a materials ability to be eroded, deposited, or transported. In PDC modelling, investigating substrate and flow interaction is pivotal in our understanding of deposit architecture [Rowley et al. 2011; Lucchi et al. 2022; Brand et al. 2023]. Here we explore the most replicable material for use in future experiments wishing to explore flows over erodible substrates (Table 5).

When exploring the behaviour of material to be used in a substrate, the angle of repose can be a representation of the shear strength [Keaton 2018; Breard et al. 2022; Dai et al. 2022]. The shear strength is the ability for a material to withstand a shear stress [Keaton 2018]. Therefore, directly correlating to the "resistance" of a material to this shear stress (i.e. whether the material is more or less likely to be moved by a force). In dry, granular material SAoR tends to be governed by particle shape [Beakawi Al-Hashemi and Baghabra Al-Amoudi 2018; Keaton 2018] and in our results we also see a strong influence from fines content (Figure 3B). This is likely to be due to a range of packing at which particle jamming occurs. For example, with the increase in fine particles, jamming also increases. Furthermore, the temporal evolution of the strain rate, for instance, can have a strong impact on where jamming occurs. The materials that most closely match the range of the pyroclastic SAoR values are cornstarch, fine sand and industrial pumice (Table 5). Ballotini 1 and 2 can be used but display lower SAoR values. This is not a problem for substrate modelling but may mean that ballotini displays a lower friction coefficient and may be more likely to be moved under shearing conditions. Analogue material may be chosen based on the parameters to be investigated. For example, in substrate experiments, a finer material such as cornstarch or ballotini 1 may be adopted. In contrast, for experiments requiring a coarser or more angular material, fine sand, industrial pumice, or ballotini 2 would make a good analogue alternative.

### 5.3.2 *Wet experiments*

*For simulating a flow*

As moisture content increases, the cohesive behaviours and resulting shear strength of both pyroclastic and analogue material changes drastically, even with the addition of small weight percentages (>0.50 wt.%). This heightened moisture can lead to a transition in flow characteristics, shifting from a state of free-flowing material (i.e. low HR, CI, SAoR and DAoR values) to that of a non-flowing material (Figure 6). With increasing moisture added to the material, SAoR, DAoR, HR and CI values increase, representing poorer flowability. This is until ~80%

Table 5: Dry pyroclastic material in comparison to analogue material for use in experiments. × is where fluidisation behaviours were present, n/a symbolises experiments that did not take place.

| Dry Experiments | Pyroclastic materials | Ballotini 1 | Ballotini 2 | Fine Sand | Cornstarch | Industrial pumice |
|---|---|---|---|---|---|---|
| HR | 1.1–1.3 | 1.0 | 1.0 | 1.1 | 1.4 | 1.2 |
| CI | 6.6–24 | 3.3 | 0.0 | 8.6 | 27.1 | 18.3 |
| SAoR | 28–43 | 17.4 | 18.8 | 30 | 37 | 30 |
| DAoR | 39–61 | 32 | 32 | 39 | 59 | 41 |
| Bubbling fluidisation | × | × | × | × | n/a | × |
| Channelling | × | – | – | – | n/a | – |
| Explosive channelling | – | – | – | – | n/a | – |
| Cracking | – | – | – | – | n/a | – |

fines content where there is a decrease in SAoR and DAoR which indicates better flowability (Figure 7). This is thought to be due to effects of interparticle lubrication or clumping of material. Cornstarch, fine sand and industrial pumice all sit well within the limits of SAoR, DAoR, HR and CI values of wet pyroclastic material used in this study (Table 6). With increasing moisture, ballotini 1 & 2 display more similar results to the pyroclastic material and also sit within the wet pyroclastic material range (Figure 7, Table 6).

Ballotini is one of the most commonly used analogue materials in experimental modelling due to its spherical properties and simple characterisation behaviours [Roche et al. 2004; Montserrat et al. 2012; Rowley et al. 2014; Smith et al. 2018; Smith et al. 2020, Table 1]. Ballotini glass beads are made of soda-lime glass and follow the Group A Geldart classification [Geldart 1973] meaning that they are non-cohesive and display homogeneous fluidisation behaviours [Smith et al. 2020]. In dry conditions, our experiments also show this behaviour, however with the addition of moisture behaviours changed drastically. A key observation made from these experiments is the effect of wetting and quick drying of ballotini beads from very small moisture levels (>0.50 wt.%). During the fluidisation experiments, it became evident that ballotini beads would "bind" together creating a strong lattice of the particles which had to be manually broken. This may be due to leaching of the coating on the ballotini or by salt-like precipitation occurring at the bonds between particles. Material in a nearly dry condition can experience greater strength due to the effect of suction [Ciantia et al. 2015] and interparticle friction factors can increase between 3.5 to 30 just by the wetting of material [Skinner 1969]. Liu et al. [2009] added small concentrations (0.3, 0.5, 0.6, 0.8 and 1.0%) of a binder liquid (water) to ballotini and created compressed pellets of materials. It was noted that an increase in binder viscosity (from water to silicone oil) and a decrease in particle size increased the overall granule strength [Liu et al. 2009]. However, this behaviour could also be due to lack of cleaning and contamination of the ballotini, as material from the supplier may be affected by contaminants on their surface. Ultimately, the origin of this ballotini behaviour is unknown. Nonetheless, the results from these experiments show that caution should be taken when (a) using ballotini in the presence of moisture in quick-drying environments, (b) preparation and cleaning of ballotini before use to remove surface contaminants and (c) if using ballotini within a moisture experiment, limit the wetting and drying of ballotini and complete experiments quickly to reduce this affect. Alternatively, this behaviour may also be utilized to take in-situ samples of material to look at internal structures.

For experiments in which moisture is being explored, fine sand and cornstarch are good substitutes and match the range of pyroclastic behaviour in wet conditions. Our recommendation is the use of fine sand because it shows similar fluidisation behaviours to the pyroclastic material. However, these materials may not adequately represent material with high fines content. Therefore, to better explore the role of fines content a combination of fine sand and cornstarch is recommended.

*For use as a substrate for flume experiments*

For substrate interaction experiments in wet environments, we again recommend fine sand and cornstarch. Ballotini 1 and 2 make strong analogues but should not be used in wet environments under quick drying (i.e. basal drying from gas flux) or left for a long period of time prior to use.

The materials used within these experiments cover a range of sizes and densities comparable to those of equivalent pyroclastic materials and exhibit similar flowability behaviours as demonstrated in the SAoR, DAoR and BTD results. In situations where pyroclastic material is limited or unsuitable for experimental modelling, it is essential to carefully select appropriate analogue materials. We recommend tailoring the choice of material to suit the specific experimental and scaling requirements, as there is no "one size fits all" material solution. By employing a series of static and dynamic experiments, we have investigated the optimal analogue materials for investigating PDC behaviour's for both the deposit and current itself. Furthermore, we examine these behaviours under varying moisture conditions. Our findings indicate that particle size, shape, sorting, and fines content profoundly influence the static and dynamic behaviours of pyroclastic materials in both dry and wet conditions.

## 6 Conclusions

Modelling pyroclastic density currents (PDCs) is a challenging, yet essential element of hazard forecasting and assessment. The dynamics within these systems are difficult to understand and observe. PDCs exist as multiphase flow and are inferred to show behaviours of various rheology under different conditions. Furthermore, PDCs are unpredictable, and internal

Table 6: Wet (0.5, 1, 2.5 wt.%) pyroclastic material in comparison to analogue material for use in experiments. × is where fluidisation behaviours were present, n/a symbolises experiments that did not take place.

| 0.5, 1, 2.5 wt.% moisture experiments | | Pyroclastic materials | Ballotini 1 | Ballotini 2 | Fine Sand | Cornstarch | Crushed pumice |
|---|---|---|---|---|---|---|---|
| HR | 0.5 | 1.1 – 1.4 | 1.20 | 1.2 | 1.2 | 1.4 | 1.2 |
| | 1 | 1.0–1.5 | 1.5 | 1.1 | 1.2 | 1.4 | 1.8 |
| | 2.5 | 1.0–1.6 | 1.5 | 1.0 | 1.2 | 1.3 | 1.2 |
| CI | 0.5 | 9.1–29 | 16.7 | 14.29 | 14.6 | 28.4 | 18.7 |
| | 1 | 5.4–35 | 33.3 | 11.8 | 15.0 | 27.3 | 15.2 |
| | 2.5 | 11–36 | 34.2 | 3.23 | 15.1 | 25 | 17.2 |
| SAoR (°) | 0.5 | 23 – 38 | 54 | 50.7 | 33 | 34 | 28 |
| | 1 | 36–54 | 54.2 | 50.3 | 54 | 46 | 36 |
| | 2.5 | 32–48 | 55 | 53.4 | 45 | 37 | 30 |
| DAoR (°) | 0.5 | 45–68 | 66 | 50.5 | 59 | 59 | 46 |
| | 1 | 49–86 | 62 | 60 | 73 | 53 | 49 |
| | 2.5 | 50–90 | 56 | 62 | 78 | 55 | 53 |
| Bubbling fluidisation | 0.5 | × | – | – | × | n/a | × |
| | 1 | × | – | – | × | n/a | × |
| | 2.5 | × | – | – | × | n/a | n/a |
| Diffusive Cracking | 0.5 | × | – | – | – | n/a | – |
| | 1 | × | – | – | – | n/a | – |
| | 2.5 | – | – | – | – | n/a | n/a |
| Channelling | 0.5 | × | – | – | – | n/a | – |
| | 1 | × | – | – | – | n/a | – |
| | 2.5 | × | – | – | – | n/a | n/a |
| Explosive Channelling | 0.5 | × | – | – | × | n/a | – |
| | 1 | × | – | – | – | n/a | × |
| | 2.5 | × | – | – | × | n/a | n/a |
| Pocketing | 0.5 | × | – | – | × | n/a | × |
| | 1 | × | – | – | × | n/a | × |
| | 2.5 | × | – | – | × | n/a | n/a |

processes are often difficult to directly measure and can be obscured by a co-ignimbrite cloud. The use of analogue experiments are an important and attractive tool for investigating the internal dynamics of PDCs. Better understanding of the fundamental physics of PDCs will lead to deeper insights into the physical properties underlying these phenomena. In turn, this will lead to the better comprehensive integration of variables into numerical equations and computational models. Missing from our current understanding, is the comparison of a wide range of pyroclastic samples with well-known analogue materials in a range of environments (i.e. static, dynamic, wet and dry).

The use of analogue experiments are an important tool for investigating internal PDC dynamics. Previous analogue experiments have ensured the removal of moisture within a material to limit the impact of moisture related cohesion. However, this does not reflect the reality of natural systems where moisture can be introduced into a PDC, such as, where temperature and pressure allow the water phase to condense and form droplets. The addition of moisture can lead to fundamental changes in material properties resulting in significant impacts on geomechanical behaviours (size, density, shear strength), fluidisation and flowability. For example, the rapid vaporisation of water into steam on PDC interaction with a wet substrate can lead to formation of a new gas source, increasing mobility and fluidisation.

Our findings explore the significant variations in behaviours of a suite of pyroclastic material under varying experimental conditions. The geomechanical properties of natural pyroclastic material are controlled by particle shape and size. Interestingly, the fines content (%) of a material has significant controls on angle of repose, fluidisation and flowability. Furthermore, the addition of moisture can greatly influence material behaviours in both static and dynamic environments and creates a package of material which is less likely to fluidise and flow. This work highlights the importance of validating the material choice used in modelling experiments, especially in wet conditions. Our findings not only enhance the fidelity of experimental models, but also offer practical guidance and values for future research endeavours in this domain.

## Author Contributions

Nemi Walding: Conceptualization, Validation, Formal analysis, Investigation, Writing—Original Draft, Visualisation. Rebecca Williams, Pete Rowley, Natasha Dowey: Conceptual-

ization, Supervision and Writing—Review and Editing. Anna Bird and Dan Parsons: Writing—Review and Editing.

## Acknowledgements

N. Walding is supported by the EU Horizon 2020 Programme (Project GEOSTICK 712525). The authors would like to thank Ulrich Kueppers, Tom Johnson, Ermanno Brosch and Gert Lube for providing the pyroclastic samples used in these experiments. We thank Jacob Nash, Mark Gilbertson and Samuel Mitchell for access to and development of the fluidisation chamber at the University of Bristol. Louis Chambers and Caitlin Malon are thanked for their assistance in the laboratory. M. Johnson and A. Richardson advised on the statistical analysis. We would like to thank Eric Breard and Ermanno Brosch for their thoughtful comments and reviews.

## Data Availability

All supplementary material (A–E) is publicly available from GitHub (https://github.com/nwalding/Walding-et-al.-2024_SupplementaryMaterial). A—Experimental methodology used in this work from Walding et al. [2023]. B—Excel Spreadsheet of all geomechanical data collected in the mechanical experiments. C—Fluidisation videos showing diffusive cracking behaviour observed in fluidisation experiments of material. Colima 0.5 wt.% moisture. Other fluidisation videos can be found in the Google Drive link on GitHub. D—Tung 1–6 fluidisation profiles from Walding et al. [2023]. E—Additional PCA data including correlation plot, scree plot and cos2 plot.

## Copyright notice



## References

Abdullah, E. and D. Geldart (1999). "The use of bulk density measurements as flowability indicators". *Powder Technology* 102(2), pages 151–165. DOI: 10.1016/s0032-5910(98)00208-3.

Alidibirov, M. and D. Dingwell (2000). "Three fragmentation mechanisms for highly viscous magma under rapid decompression". *Journal of Volcanology and Geothermal Research* 100(1–4), pages 413–421. DOI: 10.1016/s0377-0273(00)00149-9.

Amidon, G., P. Meyer, and D. Mudie (2017). "Particle, Powder, and Compact Characterization". *Developing Solid Oral Dosage Forms*. Elsevier, pages 271–293. ISBN: 9780128024478. DOI: 10.1016/b978-0-12-802447-8.00010-8.

Aravena, A., L. Chupin, T. Dubois, and O. Roche (2021). "The influence of gas pore pressure in dense granular flows: numerical simulations versus experiments and implications for pyroclastic density currents". *Bulletin of Volcanology* 83(11). DOI: 10.1007/s00445-021-01507-7.

Barclay, J., J. E. Johnstone, and A. J. Matthews (2006). "Meteorological monitoring of an active volcano: Implications for eruption prediction". *Journal of Volcanology and Geothermal Research* 150(4), pages 339–358. DOI: 10.1016/j.jvolgeores.2005.07.020.

Bardot, L. (2000). "Emplacement temperature determinations of proximal pyroclastic deposits on Santorini, Greece, and their implications". *Bulletin of Volcanology* 61(7), pages 450–467. DOI: 10.1007/pl00008911.

Bareschino, P., T. Gravina, L. Lirer, A. Marzocchella, P. Petrosino, and P. Salatino (2007). "Fluidization and de-aeration of pyroclastic mixtures: The influence of fines content, polydispersity and shear flow". *Journal of Volcanology and Geothermal Research* 164(4), pages 284–292. DOI: 10.1016/j.jvolgeores.2007.05.013.

Beakawi Al-Hashemi, H. M. and O. S. Baghabra Al-Amoudi (2018). "A review on the angle of repose of granular materials". *Powder Technology* 330, pages 397–417. DOI: 10.1016/j.powtec.2018.02.003.

Benage, M. C., J. Dufek, and P. A. Mothes (2016). "Quantifying entrainment in pyroclastic density currents from the Tungurahua eruption, Ecuador: Integrating field proxies with numerical simulations". *Geophysical Research Letters* 43(13), pages 6932–6941. DOI: 10.1002/2016gl069527.

Blott, S. J. and K. Pye (2001). "GRADISTAT: a grain size distribution and statistics package for the analysis of unconsolidated sediments". *Earth Surface Processes and Landforms* 26(11), pages 1237–1248. DOI: 10.1002/esp.261.

Brand, B. D., N. Pollock, J. W. Vallance, T. E. Ongaro, O. Roche, M. Trolese, G. Giordano, A. A. Marshall, and C. W. Criswell (2023). "Advances in our understanding of pyroclastic current behavior from the 1980 eruption sequence of Mount St. Helens volcano (Washington), USA". *Bulletin of Volcanology* 85(4). DOI: 10.1007/s00445-022-01617-w.

Branney, M. J. and P. Kokelaar (1992). "A reappraisal of ignimbrite emplacement: progressive aggradation and changes from particulate to non-particulate flow during emplacement of high-grade ignimbrite". *Bulletin of Volcanology* 54(6), pages 504–520. DOI: 10.1007/bf00301396.

– (1997). "Giant bed from a sustained catastrophic density current flowing over topography: Acatlán ignimbrite, Mexico". *Geology* 25(2), page 115. DOI: 10.1130/0091-7613(1997)025<0115:gbfasc>2.3.co;2.

– (2002). *Pyroclastic density currents and the sedimentation of ignimbrites*. Volume 27. Geological Society memoir. London: The Geological Society.

Breard, E. C. P., J. Dufek, S. Charbonnier, V. Gueugneau, T. Giachetti, and B. Walsh (2023). "The fragmentation-induced fluidisation of pyroclastic density currents". *Nature Communications* 14(1). DOI: 10.1038/s41467-023-37867-1.

Breard, E. C. P., J. Dufek, and G. Lube (2018). "Enhanced Mobility in Concentrated Pyroclastic Density Currents: An Examination of a Self-Fluidization Mechanism". *Geophysical Research Letters* 45(2), pages 654–664. DOI: 10.1002/2017gl075759.

Breard, E. C. P., L. Fullard, J. Dufek, M. Tennenbaum, A. Fernandez Nieves, and J. F. Dietiker (2022). "Investigating the rheology of fluidized and non-fluidized gas-particle beds: implications for the dynamics of geophysical flows and substrate entrainment". *Granular Matter* 24(1). DOI: 10.1007/s10035-021-01192-5.

Breard, E. C. P., J. R. Jones, L. Fullard, G. Lube, C. Davies, and J. Dufek (2019). "The Permeability of Volcanic Mixtures—Implications for Pyroclastic Currents". *Journal of Geophysical Research: Solid Earth* 124(2), pages 1343–1360. DOI: 10.1029/2018jb016544.

Breard, E. C. and G. Lube (2017). "Inside pyroclastic density currents – uncovering the enigmatic flow structure and transport behaviour in large-scale experiments". *Earth and Planetary Science Letters* 458, pages 22–36. DOI: 10.1016/j.epsl.2016.10.016.

Brosch, E., G. Lube, M. Cerminara, T. Esposti-Ongaro, E. C. P. Breard, J. Dufek, B. Sovilla, and L. Fullard (2021). "Destructiveness of pyroclastic surges controlled by turbulent fluctuations". *Nature Communications* 12(1). DOI: 10.1038/s41467-021-27517-9.

Brown, R. J., T. L. Barry, M. J. Branney, M. S. Pringle, and S. E. Bryan (2003). "The Quaternary pyroclastic succession of southeast Tenerife, Canary Islands: explosive eruptions, related caldera subsidence, and sector collapse". *Geological Magazine* 140(3), pages 265–288. DOI: 10.1017/s0016756802007252.

Brown, R. J. and M. J. Branney (2013). "Internal flow variations and diachronous sedimentation within extensive, sustained, density-stratified pyroclastic density currents flowing down gentle slopes, as revealed by the internal architectures of ignimbrites on Tenerife". *Bulletin of Volcanology* 75(7). DOI: 10.1007/s00445-013-0727-0.

Burgisser, A., G. W. Bergantz, and R. E. Breidenthal (2005). "Addressing complexity in laboratory experiments: the scaling of dilute multiphase flows in magmatic systems". *Journal of Volcanology and Geothermal Research* 141(3–4), pages 245–265. DOI: 10.1016/j.jvolgeores.2004.11.001.

Bursik, M. I. and A. W. Woods (1996). "The dynamics and thermodynamics of large ash flows". *Bulletin of Volcanology* 58(2–3), pages 175–193. DOI: 10.1007/s004450050134.

Camuffo, D. (2019). "Theoretical Grounds for Humidity". *Microclimate for Cultural Heritage*. Elsevier, pages 43–59. ISBN: 9780444641069. DOI: 10.1016/b978-0-444-64106-9.00003-1.

Cas, R. A. F. and J. V. Wright (1988). "Modern pyroclastic fall deposits and their eruptions". *Volcanic Successions Modern and Ancient*. Springer Netherlands, pages 128–174. ISBN: 9789400931671. DOI: 10.1007/978-94-009-3167-1_6.

Cas, R. A. and J. V. Wright (1991). "Subaqueous pyroclastic flows and ignimbrites: an assessment". *Bulletin of Volcanology* 53(5), pages 357–380. DOI: 10.1007/bf00280227.

Chedeville, C. and O. Roche (2014). "Autofluidization of pyroclastic flows propagating on rough substrates as shown by laboratory experiments". *Journal of Geophysical Research: Solid Earth* 119(3), pages 1764–1776. DOI: 10.1002/2013jb010554.

Chen, D., J. Zheng, C. Zhang, D. Guan, Y. Li, and Y. Wang (2021). "Critical Shear Stress for Erosion of Sand-Mud Mixtures and Pure Mud". *Frontiers in Marine Science* 8. DOI: 10.3389/fmars.2021.713039.

Chen, J., R. Gao, and Y. Liu (2019). "Numerical Study of Particle Morphology Effect on the Angle of Repose for Coarse Assemblies Using DEM". *Advances in Materials Science and Engineering* 2019, pages 1–15. DOI: 10.1155/2019/8095267.

Ciantia, M. O., R. Castellanza, G. B. Crosta, and T. Hueckel (2015). "Effects of mineral suspension and dissolution on strength and compressibility of soft carbonate rocks". *Engineering Geology* 184, pages 1–18. DOI: 10.1016/j.enggeo.2014.10.024.

Cioni, R., L. Gurioli, R. Lanza, and E. Zanella (2004). "Temperatures of the A.D. 79 pyroclastic density current deposits (Vesuvius, Italy)". *Journal of Geophysical Research: Solid Earth* 109(B2). DOI: 10.1029/2002jb002251.

Cioni, R., M. Pistolesi, and M. Rosi (2015). "Plinian and Subplinian Eruptions". *The Encyclopedia of Volcanoes*. Elsevier, pages 519–535. ISBN: 9780123859389. DOI: 10.1016/b978-0-12-385938-9.00029-8.

Cocco, R. and J. W. Chew (2023). "50 years of Geldart classification". *Powder Technology* 428, page 118861. DOI: 10.1016/j.powtec.2023.118861.

Cole, P. D., E. S. Calder, T. H. Druitt, R. Hoblitt, R. Robertson, R. S. J. Sparks, and S. R. Young (1998). "Pyroclastic flows generated by gravitational instability of the 1996–97 Lava Dome of Soufriere Hills Volcano, Montserrat". *Geophysical Research Letters* 25(18), pages 3425–3428. DOI: 10.1029/98gl01510.

Cole, P. D., E. S. Calder, R. S. J. Sparks, A. B. Clarke, T. H. Druitt, S. R. Young, R. A. Herd, C. L. Harford, and G. E. Norton (2002). "Deposits from dome-collapse and fountain-collapse pyroclastic flows at Soufrière Hills Volcano, Montserrat". *Geological Society, London, Memoirs* 21(1), pages 231–262. DOI: 10.1144/gsl.mem.2002.021.01.11.

Dai, B.-B., T.-Q. Li, L.-J. Deng, J. Yang, and W.-H. Yuan (2022). "Fabric effect on the angle of repose in granular materials". *Powder Technology* 400, page 117256. DOI: 10.1016/j.powtec.2022.117256.

Dartevelle, S., W. I. Rose, J. Stix, K. Kelfoun, and J. W. Vallance (2004). "Numerical modeling of geophysical granular flows: 2. Computer simulations of plinian clouds and pyroclastic flows and surges". *Geochemistry, Geophysics, Geosystems* 5(8). DOI: 10.1029/2003gc000637.

Dellino, P., R. Büttner, F. Dioguardi, D. M. Doronzo, L. La Volpe, D. Mele, I. Sonder, R. Sulpizio, and B. Zimanowski (2010). "Experimental evidence links volcanic particle characteristics to pyroclastic flow hazard". *Earth and Planetary Science Letters* 295(1–2), pages 314–320. DOI: 10.1016/j.epsl.2010.04.022.

Dellino, P., B. Zimanowski, R. Büttner, L. La Volpe, D. Mele, and R. Sulpizio (2007). "Large-scale experiments on the mechanics of pyroclastic flows: Design, engineering, and first

results". *Journal of Geophysical Research: Solid Earth* 112(B4). DOI: 10.1029/2006jb004313.

Douillet, G. A., B. Bernard, M. Bouysson, Q. Chaffaut, D. B. Dingwell, L. Gegg, I. Hoelscher, U. Kueppers, C. Mato, V. A. Ritz, F. Schlunegger, and P. Witting (2018). "Pyroclastic dune bedforms: macroscale structures and lateral variations. Examples from the 2006 pyroclastic currents at Tungurahua (Ecuador)". *Sedimentology* 66(5), pages 1531–1559. DOI: 10.1111/sed.12542.

Douillet, G. A., È. Tsang-Hin-Sun, U. Kueppers, J. Letort, D. A. Pacheco, F. Goldstein, F. Von Aulock, Y. Lavallée, J. B. Hanson, J. Bustillos, C. Robin, P. Ramón, M. Hall, and D. B. Dingwell (2013). "Sedimentology and geomorphology of the deposits from the August 2006 pyroclastic density currents at Tungurahua volcano, Ecuador". *Bulletin of Volcanology* 75(11). DOI: 10.1007/s00445-013-0765-7.

Doyle, E., A. Hogg, H. Mader, and R. Sparks (2010). "A two-layer model for the evolution and propagation of dense and dilute regions of pyroclastic currents". *Journal of Volcanology and Geothermal Research* 190(3–4), pages 365–378. DOI: 10.1016/j.jvolgeores.2009.12.004.

Druitt, T. H., G. Avard, G. Bruni, P. Lettieri, and F. Maez (2007). "Gas retention in fine-grained pyroclastic flow materials at high temperatures". *Bulletin of Volcanology* 69(8), pages 881–901. DOI: 10.1007/s00445-007-0116-7.

Duane, W. J., N. C. Pepin, M. L. Losleben, and D. R. Hardy (2008). "General Characteristics of Temperature and Humidity Variability on Kilimanjaro, Tanzania". *Arctic, Antarctic, and Alpine Research* 40(2), pages 323–334. DOI: 10.1657/1523-0430(06-127)[duane]2.0.co;2.

Dufek, J. and M. Manga (2008). "In situ production of ash in pyroclastic flows". *Journal of Geophysical Research: Solid Earth* 113(B9). DOI: 10.1029/2007jb005555.

Dufek, J. (2016). "The Fluid Mechanics of Pyroclastic Density Currents". *Annual Review of Fluid Mechanics* 48(1), pages 459–485. DOI: 10.1146/annurev-fluid-122414-034252.

Dury, C. M., G. H. Ristow, J. L. Moss, and M. Nakagawa (1998). "Boundary effects on the angle of repose in rotating cylinders". *Physical Review E* 57(4), pages 4491–4497. DOI: 10.1103/physreve.57.4491.

Esposti Ongaro, T., N. A., T. M., and M. G. (2002). "Pyroclastic flow hazard assessment at Vesuvius (Italy) by using numerical modeling. II. Analysis of flow variables". *Bulletin of Volcanology* 64(3–4), pages 178–191. DOI: 10.1007/s00445-001-0190-1.

Esposti Ongaro, T., A. B. Clarke, B. Voight, A. Neri, and C. Widiwijayanti (2012). "Multiphase flow dynamics of pyroclastic density currents during the May 18, 1980 lateral blast of Mount St. Helens". *Journal of Geophysical Research: Solid Earth* 117(B6). DOI: 10.1029/2011jb009081.

Esposti Ongaro, T., S. Barsotti, A. Neri, and M. V. Salvetti (2011). "Large-eddy simulation of pyroclastic density currents". *Quality and Reliability of Large-Eddy Simulations II*. Springer Netherlands, pages 161–170. ISBN: 9789400702318. DOI: 10.1007/978-94-007-0231-8_15.

Eychenne, J., J.-L. Le Pennec, L. Troncoso, M. Gouhier, and J.-M. Nedelec (2012). "Causes and consequences of bimodal grain-size distribution of tephra fall deposited during the August 2006 Tungurahua eruption (Ecuador)". *Bulletin of Volcanology* 74(1), pages 187–205. DOI: 10.1007/s00445-011-0517-5.

Fisher, R. V. (1979). "Models for pyroclastic surges and pyroclastic flows". *Journal of Volcanology and Geothermal Research* 6(3–4), pages 305–318. DOI: 10.1016/0377-0273(79)90008-8.

Fisher, R. V. and H.-U. Schmincke (1984). "Pyroclastic Flow Deposits". *Pyroclastic Rocks*. Springer Berlin Heidelberg, pages 186–230. ISBN: 9783642748646. DOI: 10.1007/978-3-642-74864-6_8.

Gauthier, T. D. (2001). "Detecting Trends Using Spearman's Rank Correlation Coefficient". *Environmental Forensics* 2(4), pages 359–362. DOI: 10.1080/713848278.

Geldart, D. (1973). "Types of gas fluidization". *Powder Technology* 7(5), pages 285–292. DOI: 10.1016/0032-5910(73)80037-3.

Gilbertson, M. A., A. Taylor, S. J. Mitchell, and A. C. Rust (2020). "A Fluidisation Mechanism for Secondary Hydroeruptions in Pyroclastic Flow Deposits". *Frontiers in Earth Science* 8. DOI: 10.3389/feart.2020.00324.

Gorle, A. P. and S. S. Chopade (2020). "Liquisolid Technology: Preparation, Characterization and Applications". *Journal of Drug Delivery and Therapeutics* 10(3-s), pages 295–307. DOI: 10.22270/jddt.v10i3-s.4067.

Hall, M. L., A. L. Steele, P. A. Mothes, and M. C. Ruiz (2013). "Pyroclastic density currents (PDC) of the 16–17 August 2006 eruptions of Tungurahua volcano, Ecuador: Geophysical registry and characteristics". *Journal of Volcanology and Geothermal Research* 265, pages 78–93. DOI: 10.1016/j.jvolgeores.2013.08.011.

Hartmann, D. L. (2016). *Global Physical Climatology*. 2nd Edition. Volume 103. Elsevier. ISBN: 9780123285317. DOI: 10.1016/c2009-0-00030-0.

Huang, Q., H. Zhang, and J. Zhu (2009). "Experimental study on fluidization of fine powders in rotating drums with various wall friction and baffled rotating drums". *Chemical Engineering Science* 64(9), pages 2234–2244. DOI: 10.1016/j.ces.2009.01.047.

Inman, D. L. (1952). "Measures for Describing the Size Distribution of Sediments". *SEPM Journal of Sedimentary Research* Vol. 22. DOI: 10.1306/d42694db-2b26-11d7-8648000102c1865d.

Kassambara, A. and F. Mundt (2016). *factoextra: Extract and Visualize the Results of Multivariate Data Analyses*. DOI: 10.32614/cran.package.factoextra.

Keaton, J. R. (2018). "Angle of Internal Friction". *Encyclopedia of Engineering Geology*. Springer International Publishing, pages 22–23. ISBN: 9783319735689. DOI: 10.1007/978-3-319-73568-9_16.

Kelfoun, K., V. Gueugneau, J.-C. Komorowski, N. Aisyah, N. Cholik, and C. Merciecca (2017). "Simulation of block-and-ash flows and ash-cloud surges of the 2010 eruption of Merapi volcano with a two-layer model". *Journal of Geophysical Research: Solid Earth* 122(6), pages 4277–4292. DOI: 10.1002/2017jb013981.

Kelfoun, K., P. Samaniego, P. Palacios, and D. Barba (2009). "Testing the suitability of frictional behaviour for pyroclastic flow simulation by comparison with a well-constrained eruption at Tungurahua volcano (Ecuador)". *Bulletin of Volcanology* 71(9), pages 1057–1075. DOI: 10.1007/s00445-009-0286-6.

Kim, T.-H. and C. Hwang (2003). "Modeling of tensile strength on moist granular earth material at low water content". *Engineering Geology* 69(3–4), pages 233–244. DOI: 10.1016/s0013-7952(02)00284-3.

Kim, T.-H. and S. Sture (2008). "Capillary-induced tensile strength in unsaturated sands". *Canadian Geotechnical Journal* 45(5), pages 726–737. DOI: 10.1139/t08-017.

Kubo Hutchison, A. and J. Dufek (2021). "Generation of Overspill Pyroclastic Density Currents in Sinuous Channels". *Journal of Geophysical Research: Solid Earth* 126(10). DOI: 10.1029/2021jb022442.

LaMarche, C. Q., A. W. Miller, P. Liu, and C. M. Hrenya (2016). "Linking micro-scale predictions of capillary forces to macro-scale fluidization experiments in humid environments". *AIChE Journal* 62(10), pages 3585–3597. DOI: 10.1002/aic.15281.

Lê, S., J. Josse, and F. Husson (2008). "FactoMineR: AnRPackage for Multivariate Analysis". *Journal of Statistical Software* 25(1). DOI: 10.18637/jss.v025.i01.

Lesti, C., M. Porreca, G. Giordano, M. Mattei, R. A. F. Cas, H. M. N. Wright, C. B. Folkes, and J. Viramonte (2011). "High-temperature emplacement of the Cerro Galán and Toconquis Group ignimbrites (Puna plateau, NW Argentina) determined by TRM analyses". *Bulletin of Volcanology* 73(10), pages 1535–1565. DOI: 10.1007/s00445-011-0536-2.

Leturia, M., M. Benali, S. Lagarde, I. Ronga, and K. Saleh (2014). "Characterization of flow properties of cohesive powders: A comparative study of traditional and new testing methods". *Powder Technology* 253, pages 406–423. DOI: 10.1016/j.powtec.2013.11.045.

Li, W. C., G. Deng, X. Q. Liang, X. X. Sun, S. W. Wang, and M. L. Lee (2020). "Effects of stress state and fine fraction on stress transmission in internally unstable granular mixtures investigated via discrete element method". *Powder Technology* 367, pages 659–670. DOI: 10.1016/j.powtec.2020.04.024.

Lipman, P. W. (2018). "When ignimbrite meets water: Megascale gas-escape structures formed during welding". *Geology* 47(1), pages 63–66. DOI: 10.1130/g45772.1.

Liu, L., R. Smith, and J. Litster (2009). "Wet granule breakage in a breakage only high-hear mixer: Effect of formulation properties on breakage behaviour". *Powder Technology* 189(2), pages 158–164. DOI: 10.1016/j.powtec.2008.04.029.

Liu, Y., R. Gao, and J. Chen (2019). "Exploring the influence of sphericity on the mechanical behaviors of ballast particles subjected to direct shear". *Granular Matter* 21(4). DOI: 10.1007/s10035-019-0943-1.

Lowes, T. M. and M. G. Perry (1965). "The measurement of cohesion in powders". *Rheologica Acta* 4(3), pages 166–170. DOI: 10.1007/bf01969252.

Lube, G., E. C. P. Breard, S. J. Cronin, and J. Jones (2015). "Synthesizing large-scale pyroclastic flows: Experimental design, scaling, and first results from PELE". *Journal of Geophysical Research: Solid Earth* 120(3), pages 1487–1502. DOI: 10.1002/2014jb011666.

Lube, G., E. C. P. Breard, T. Esposti-Ongaro, J. Dufek, and B. Brand (2020). "Multiphase flow behaviour and hazard prediction of pyroclastic density currents". *Nature Reviews Earth & Environment* 1(7), pages 348–365. DOI: 10.1038/s43017-020-0064-8.

Lube, G., E. C. P. Breard, J. Jones, L. Fullard, J. Dufek, S. J. Cronin, and T. Wang (2019). "Generation of air lubrication within pyroclastic density currents". *Nature Geoscience* 12(5), pages 381–386. DOI: 10.1038/s41561-019-0338-2.

Lucchi, F., R. Sulpizio, S. Meschiari, C. Tranne, P. Albert, D. Mele, and P. Dellino (2022). "Sedimentological analysis of ash-rich pyroclastic density currents, with special emphasis on sin-depositional erosion and clast incorporation: The Brown Tuff eruptions (Vulcano, Italy)". *Sedimentary Geology* 427, page 106040. DOI: 10.1016/j.sedgeo.2021.106040.

McClelland, E. A. and T. H. Druitt (1989). "Palaeomagnetic estimates of emplacement temperatures of pyroclastic deposits on Santorini, Greece". *Bulletin of Volcanology* 51(1), pages 16–27. DOI: 10.1007/bf01086758.

McPhie, J., G. P. L. Walker, and R. L. Christiansen (1990). "Phreatomagmatic and phreatic fall and surge deposits from explosions at Kilauea volcano, Hawaii, 1790 a.d.: Keanakakoi Ash Member". *Bulletin of Volcanology* 52(5), pages 334–354. DOI: 10.1007/bf00302047.

Mirabella, A., M. Egli, S. Raimondi, and D. Giaccai (2005). "Origin of Clay Minerals in Soils on Pyroclastic Deposits in the Island of Lipari (Italy)". *Clays and Clay Minerals* 53(4), pages 409–421. DOI: 10.1346/ccmn.2005.0530409.

Montserrat, S., A. Tamburrino, O. Roche, and Y. Niño (2012). "Pore fluid pressure diffusion in defluidizing granular columns". *Journal of Geophysical Research: Earth Surface* 117(F2). DOI: 10.1029/2011jf002164.

Moondra, S., R. Maheshwari, N. Taneja, M. Tekade, and R. K. Tekadle (2018). "Bulk Level Properties and its Role in Formulation Development and Processing". *Dosage Form Design Parameters*. Elsevier, pages 221–256. ISBN: 9780128144213. DOI: 10.1016/b978-0-12-814421-3.00006-3.

Morrissey, M. and L. G. Mastin (2000). "Vulcanian Eruptions". *The Encyclopedia of Volcanoes*. Edited by H. Sigurdsson. 1st Edition. San Diego, CA: Academic Press, pages 463–475.

Moyer, T. C. and D. A. Swanson (1987). "Secondary hydroeruptions in pyroclastic-flow deposits: Examples from Mount St. Helens". *Journal of Volcanology and Geothermal Research* 32(4), pages 299–319. DOI: 10.1016/0377-0273(87)90081-3.

Nagasawa, K. (1978). "Chapter 2 Weathering of volcanic ash and other pyroclastic materials". *Clays and Clay Minerals of Japan*. Elsevier, pages 105–125. DOI: 10.1016/s0070-4571(08)70683-6.

Osman, S., M. Thomas, J. Crummy, and S. Carver (2022). "Investigation of geomechanical properties of tephra rele-

vant to roof loading for application in vulnerability analyses". *Journal of Applied Volcanology* 11(1). DOI: 10.1186/s13617-022-00121-2.

Pacheco-Hoyos, J. G., G. J. Aguirre-Díaz, and P. Dávila-Harris (2020). "Elutriation pipes in ignimbrites: An analysis of concepts based on the Huichapan Ignimbrite, Mexico". *Journal of Volcanology and Geothermal Research* 403, page 107026. DOI: 10.1016/j.jvolgeores.2020.107026.

Pardo, N., S. J. Cronin, K. Németh, M. Brenna, C. I. Schipper, E. Breard, J. D. White, J. Procter, B. Stewart, J. Agustín-Flores, A. Moebis, A. Zernack, G. Kereszturi, G. Lube, A. Auer, V. Neall, and C. Wallace (2014). "Perils in distinguishing phreatic from phreatomagmatic ash; insights into the eruption mechanisms of the 6 August 2012 Mt. Tongariro eruption, New Zealand". *Journal of Volcanology and Geothermal Research* 286, pages 397–414. DOI: 10.1016/j.jvolgeores.2014.05.001.

Pensa, A., G. Giordano, S. Corrado, and P. P. Petrone (2023). "A new hazard scenario at Vesuvius: deadly thermal impact of detached ash cloud surges in 79CE at Herculaneum". *Scientific Reports* 13(1). DOI: 10.1038/s41598-023-32623-3.

Pepin, N. C., G. Pike, M. Schaefer, C. M. Boston, and H. Lovell (2017). "A comparison of simultaneous temperature and humidity observations from the SW and NE slopes of Kilimanjaro: The role of slope aspect and differential land-cover in controlling mountain climate". *Global and Planetary Change* 157, pages 244–258. DOI: 10.1016/j.gloplacha.2017.08.006.

Pierrat, P. and H. S. Caram (1997). "Tensile strength of wet granula materials". *Powder Technology* 91(2), pages 83–93. DOI: 10.1016/s0032-5910(96)03179-8.

Roche, O., T. Druitt, and R. Cas (2001). "Experimental aqueous fluidization of ignimbrite". *Journal of Volcanology and Geothermal Research* 112(1–4), pages 267–280. DOI: 10.1016/s0377-0273(01)00246-3.

Roche, O., M. A. Gilbertson, J. C. Phillips, and R. S. J. Sparks (2004). "Experimental study of gas-fluidized granular flows with implications for pyroclastic flow emplacement". *Journal of Geophysical Research: Solid Earth* 109(B10). DOI: 10.1029/2003jb002916.

Roche, O., S. Montserrat, Y. Niño, and A. Tamburrino (2010). "Pore fluid pressure and internal kinematics of gravitational laboratory air-particle flows: Insights into the emplacement dynamics of pyroclastic flows". *Journal of Geophysical Research: Solid Earth* 115(B9). DOI: 10.1029/2009jb007133.

Roche, O. (2012). "Depositional processes and gas pore pressure in pyroclastic flows: an experimental perspective". *Bulletin of Volcanology* 74(8), pages 1807–1820. DOI: 10.1007/s00445-012-0639-4.

Rowley, P. J., P. Kokelaar, M. Menzies, and D. Waltham (2011). "Shear-Derived Mixing In Dense Granular Flows". *Journal of Sedimentary Research* 81(12), pages 874–884. DOI: 10.2110/jsr.2011.72.

Rowley, P. J., O. Roche, T. H. Druitt, and R. Cas (2014). "Experimental study of dense pyroclastic density currents using sustained, gas-fluidized granular flows". *Bulletin of Volcanology* 76(9). DOI: 10.1007/s00445-014-0855-1.

Salatino, P., P. Bareschino, A. Marzocchella, and P. Petrosino (2024). "Fluidization in pyroclastic flows". *Powder Technology* 439, page 119685. DOI: 10.1016/j.powtec.2024.119685.

Scharff, L., M. Hort, and N. R. Varley (2019). "First in-situ observation of a moving natural pyroclastic density current using Doppler radar". *Scientific Reports* 9(1). DOI: 10.1038/s41598-019-43620-w.

Schneider, C. A., W. S. Rasband, and K. W. Eliceiri (2012). "NIH Image to ImageJ: 25 years of image analysis". *Nature Methods* 9(7), pages 671–675. DOI: 10.1038/nmeth.2089.

Self, S. and R. S. J. Sparks (1978). "Characteristics of widespread pyroclastic deposits formed by the interaction of silicic magma and water". *Bulletin Volcanologique* 41(3), pages 196–212. DOI: 10.1007/bf02597223.

Skinner, A. E. (1969). "A Note on the Influence of Interparticle Friction on the Shearing Strength of a Random Assembly of Spherical Particles". *Géotechnique* 19(1), pages 150–157. DOI: 10.1680/geot.1969.19.1.150.

Smith, G., P. Rowley, R. Williams, G. Giordano, M. Trolese, A. Silleni, D. R. Parsons, and S. Capon (2020). "A bedform phase diagram for dense granular currents". *Nature Communications* 11(1). DOI: 10.1038/s41467-020-16657-z.

Smith, G. M., R. Williams, P. J. Rowley, and D. R. Parsons (2018). "Investigation of variable aeration of monodisperse mixtures: implications for pyroclastic density currents". *Bulletin of Volcanology* 80(8). DOI: 10.1007/s00445-018-1241-1.

Smith, N. J. and B. P. Kokelaar (2013). "Proximal record of the 273 ka Poris caldera-forming eruption, Las Cañadas, Tenerife". *Bulletin of Volcanology* 75(11). DOI: 10.1007/s00445-013-0768-4.

Sparks, R. S. J. (1976). "Grain size variations in ignimbrites and implications for the transport of pyroclastic flows". *Sedimentology* 23(2), pages 147–188. DOI: 10.1111/j.1365-3091.1976.tb00045.x.

– (1978). "Gas release rates from pyroclastic flows: a assessment of the role of fluidisation in their emplacement". *Bulletin Volcanologique* 41(1), pages 1–9. DOI: 10.1007/bf02597679.

Sparks, R. S. J. and C. J. N. Wilson (1990). "The Minoan Deposits: a Review of their Characteristics and Interpretation". *Thera and the Aegean World III: proceedings of the Third International Congress, Santorini, Greece, 3-9 September 1989*. Edited by D. A. Hardy. London: Thera Foundation, pages 89–99.

Team, R. C. (2023). *R: A Language and Environment for Statistical. Computing*. R Foundation for Statistical Computing, Vienna, Austria. URL: https://www.R-project.org.

Torres, R. C., S. Self, and M. M. L. Martinez (1996). "Secondary pyroclastic flows from the June 15, 1991, ignimbrite of Mount Pinatubo". *Fire and Mud: Eruptions and Lahars of Mount Pinatubo, Philippines*. Quezon City: Philippine Institute of Volcanology and Seismology, pages 351–370.

Vale, A. B., L. T. Jenkins, J. C. Phillips, A. C. Rust, A. J. Hogg, G. Kilgour, and A. Seward (2024). "Heat Transfer in Pyroclastic Density Current-Ice Interactions: Insights From Experimen-

tal and Numerical Simulations". *Journal of Geophysical Research: Solid Earth* 129(6). DOI: 10.1029/2024jb029321.

Valentine, G. A. (1987). "Stratified flow in pyroclastic surges". *Bulletin of Volcanology* 49(4), pages 616–630. DOI: 10.1007/bf01079967.

Valverde, J. M. and C. Soria-Hoyo (2015). "Vibration-induced dynamical weakening of pyroclastic flows: Insights from rotating drum experiments". *Journal of Geophysical Research: Solid Earth* 120(9), pages 6182–6190. DOI: 10.1002/2015jb012317.

Van Eaton, A. R. and C. J. Wilson (2012). "What is the role of pyroclastic density currents in volcanic ash aggregation? Perspectives from a phreatoplinian eruption deposit, New Zealand". *AGU Fall Meeting Abstracts*. Volume 2012, V41B-2789, V41B–2789.

Vecino, M. C. D., E. Rossi, V. Freret-Lorgeril, A. Fries, P. Gabellini, J. Lemus, S. Pollastri, A. P. Poulidis, M. Iguchi, and C. Bonadonna (2022). "Aerodynamic characteristics and genesis of aggregates at Sakurajima Volcano, Japan". *Scientific Reports* 12(1). DOI: 10.1038/s41598-022-05854-z.

Walding, N., R. Williams, P. Rowley, and N. Dowey (2023). "Cohesional behaviours in pyroclastic material and the implications for deposit architecture". *Bulletin of Volcanology* 85(11). DOI: 10.1007/s00445-023-01682-9.

Whelley, P. L., J. Jay, E. S. Calder, M. E. Pritchard, N. J. Cassidy, S. Alcaraz, and A. Pavez (2012). "Post-depositional fracturing and subsidence of pumice flow deposits: Lascar Volcano, Chile". *Bulletin of Volcanology* 74(2), pages 511–531. DOI: 10.1007/s00445-011-0545-1.

Wickham, H. (2009). *ggplot2: Elegant Graphics for Data Analysis*. 1st edition. Springer New York. ISBN: 9780387981413. DOI: 10.1007/978-0-387-98141-3.

Wilson, C. J. N. (1985). "The Taupo eruption, New Zealand. II. The Taupo ignimbrite". *Philosophical Transactions of the Royal Society of London. Series A, Mathematical and Physical Sciences* 314, pages 229–310. DOI: https://doi.org/10.1098/rsta.1985.0020.

– (1984). "The role of fluidization in the emplacement of pyroclastic flows, 2: Experimental results and their interpretation". *Journal of Volcanology and Geothermal Research* 20(1–2), pages 55–84. DOI: 10.1016/0377-0273(84)90066-0.

– (1980). "The role of fluidization in the emplacement of pyroclastic claws: An experimental approach". *Journal of Volcanology and Geothermal Research* 8(2–4), pages 231–249. DOI: 10.1016/0377-0273(80)90106-7.

Wilson, G., T. Wilson, N. Deligne, and J. Cole (2014). "Volcanic hazard impacts to critical infrastructure: A review". *Journal of Volcanology and Geothermal Research* 286, pages 148–182. DOI: 10.1016/j.jvolgeores.2014.08.030.

Yamamoto, T., Y. Nakamura, and H. Glicken (1999). "Pyroclastic density current from the 1888 phreatic eruption of Bandai volcano, NE Japan". *Journal of Volcanology and Geothermal Research* 90(3–4), pages 191–207. DOI: 10.1016/s0377-0273(99)00025-6.

Yu, A. and J. Hall (1994). "Packing of fine powders subjected to tapping". *Powder Technology* 78(3), pages 247–256. DOI: 10.1016/0032-5910(93)02790-h.

Zhou, X., K. Kuiper, J. Wijbrans, K. Boehm, and P. Vroon (2021). "Eruptive history and $^{40}Ar/^{39}Ar$ geochronology of the Milos volcanic field, Greece". *Geochronology* 3(1), pages 273–297. DOI: 10.5194/gchron-3-273-2021.

Zhou, Y., B. Xu, A. Yu, and P. Zulli (2002). "An experimental and numerical study of the angle of repose of coarse spheres". *Powder Technology* 125(1), pages 45–54. DOI: 10.1016/s0032-5910(01)00520-4.

Zimanowski, B., R. Büttner, V. Lorenz, and H.-G. Häfele (1997). "Fragmentation of basaltic melt in the course of explosive volcanism". *Journal of Geophysical Research: Solid Earth* 102(B1), pages 803–814. DOI: 10.1029/96jb02935.